Chemical Geology 662 (2024) 122239

Contents lists available at ScienceDirect

Chemical Geology

journal homepage: www.elsevier.com/locate/chemgeo

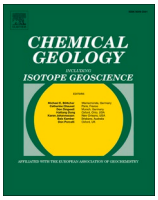

Geochemistry of carbonate microbialites through time and space: Insights from the microbialite collection of the *Muséum National d'Histoire Naturelle (MNHN)*, France

Laurane Fogret [a,*], Pierre Sansjofre [a], Stefan V. Lalonde [b]

[a] UMR7590 Institute for Mineralogy, Physics of Materials and Cosmochemistry, Muséum National d'Histoire Naturelle, Sorbonne Université, 75005 Paris, France
[b] CNRS - UMR6538 Laboratoire Geo-Ocean, European Institute for Marine Studies, Université de Bretagne Occidentale, 29280 Plouzané, France

ARTICLE INFO

Editor: Hailiang Dong

Keywords:
Microbialite
Stromatolite
Geochemistry
Paleoenvironments
Museum collection
Sample Curation

ABSTRACT

Microbialites are microbial sedimentary structures that constitute some of the oldest traces of life on Earth. By their deposition in a wide range of sedimentary environments and their presence throughout most of geological time, the sedimentological and geochemical signatures they preserve represent important paleoenvironmental archives for understanding Earth's biological and geochemical co-evolution. Here we present a large microbialite collection containing >1370 curated specimens, covering all continents except Antarctica and spanning >3.5 Ga of Earth history, that is accessible to the international scientific community for examination and sampling at the *Muséum National d'Histoire Naturelle* (MNHN) in Paris, France. After cataloguing and evaluating the samples for their lithology, biogenicity, and inferred depositional environments, we characterized the collection for selected geochemical parameters, notably carbonate stable carbon and oxygen isotope ratios, as well as major, trace, and rare earth element compositions. Finally, we explore the different geochemical proxies analyzed with regards to their utility for reconstructing evolving Earth surface environments and/or microbial metabolisms via comparison of geochemical data from the MNHN Microbialite Collection to a compilation of similar proxy data for carbonates worldwide. We demonstrate that certain temporal trends previously recognized in carbonates worldwide (e.g., with respect to variations in C and O stable isotope compositions and redox sensitive trace element enrichments) are well reflected in this collection. Our findings highlight the utility of the MNHN Microbialite Collection and microbialites more generally for reconstructing the conditions associated with habitable environments in deep time and for tracing the response of microbial communities to the geochemical evolution of Earth's surface.

1. Introduction

1.1. Microbialites: sediments demonstrating microbial influence

Microbialites are organo-sedimentary deposits where the presence or activity of microbes leads to distinct sedimentary structures that can be recognized as microbial in origin (Kalkowsky, 1908; Awramik and Margulis, 1974; Semikhatov et al., 1979). They are found in a wide variety of aqueous environments, ranging from near-freezing (Last et al., 2013) to the upper temperature limits of photosynthesis (Brock, 1978; Ward et al., 1998), at high altitudes (Farías et al., 2013; Wilmeth et al., 2021) and under as much as tens of meters of water (Bartley et al., 2015; Pratt, 2000), from freshwater (Gischler et al., 2008; Pacton et al., 2016) to hypersaline waters (D'Amelio et al., 1989; Dupraz and Visscher, 2005; Petrash et al., 2012), from highly productive waters (Armienta et al., 2008) to slow growing desert crusts and endolithic nutrient- or water-limited habitats (Bonilla-Rosso et al., 2012; Thomazo et al., 2020).

While the microorganisms responsible for microbialite formation are rarely preserved in the sedimentary record (Riding, 2000; Shapiro, 2007), they leave important mineralogical, chemical, and sedimentary traces of their presence and activity. Microbes may produce significant environmental shifts in redox and alkalinity conditions at a variety of scales: from the cell surface to the scale of mineral grains, or sediment porewaters, and even up to local water column and basinal scales (Dupraz et al., 2009; see also Dong et al., 2022 for a review). Their metabolic activity often drives the precipitation of a variety of minerals,

* Corresponding author.
E-mail address: laurane.fogret@mnhn.fr (L. Fogret).

https://doi.org/10.1016/j.chemgeo.2024.122239
Received 20 February 2024; Received in revised form 14 June 2024; Accepted 17 June 2024
Available online 19 June 2024

including phosphate and sulfide minerals, iron oxides, and most commonly, carbonates. The latter mainly result from photosynthetic uptake of CO_2 and corresponding increased alkalinity in photic environments, or by sulfate reduction in anoxic pore-water sediments or water-columns (Visscher et al., 2000; Dupraz et al., 2009). Microbialites are often, but not always, based on photosynthetic primary producers, seeking light to perform photosynthesis, and thus generating microbial sedimentary structures that are often observed growing in the direction of sunlight (Awramik and Vanyo, 1986; Bosak et al., 2009; Ojakangas et al., 2023). Microbialites may also include small algae, fungi, protozoa, and viruses (White et al., 2018; White et al., 2021). Much of the organic matter produced by the uppermost photosynthetic communities is consumed in lower layers where anaerobic bacteria and archaea dominate (Golubic, 1976; Papineau et al., 2005; Foster and Green, 2011). Examples exist of microbial populations growing without important photosynthetic contributions; e.g., under dark conditions in caves or deep waters, often fueled by lithoautotrophic sulfur-oxidizing metabolisms (Reitner, 1993; Macalady et al., 2008).

Microbialite formation testifies to ecological interactions but is not simply the result of microbial metabolic activity. Extra-polymeric substances (EPS) produced by microbial mats may also mediate lithification by surface complexation reactions (Chafetz and Buczynski, 1992; Knoll, 2003; Decho et al., 2005). Furthermore, the lack of correlation between carbon fixation rates and biogenic carbonate precipitation suggests that autotrophy may not have a major role (Wilmeth et al., 2018) and that precipitation may be primarily influenced by (pore)water chemistry changes independently of microbial activity (Dupraz et al., 2009; Hu et al., 2023). The physical process of trapping and binding of detrital sediment grains is also often important for microbialite morphogenesis (Logan, 1961; Riding and Awramik, 2000). In sum, different sedimentation modes, environmental conditions, evolving microbial community activity and composition, and early diagenetic reactions all interact to give rise to a large variety of structures that are all considered microbialites. They are generally convex upwards but can adopt a wide variety of macrostructures (Fig. 1). They are typically classified according to their mesostructural components (Fig. 1; Grey and Awramik, 2020), leading to several broad sub-categories comprised of stromatolites, dendrolites, thrombolites, leiolites, and MISS (i.e., microbially induced sedimentary structures in siliclastic sediments; Noffke, 2009). Some authors also consider, more broadly, the TSTs (i.e., tufa, sinter, travertine, and other probable microbially produced structures; de Wet and Davis, 2010) as universally microbial in origin, although this is the subject of ongoing research.

Recognizing microbial influence on sedimentation and cementation is not always straightforward. For example, some sedimentary structures commonly considered as stromatolites may be composed largely of sparry carbonate crusts of primarily abiotic origin, whereas others may take a hybrid form with alternations between microbially-influenced fine-grained laminae and sparry inorganic precipitates, blurring the line between biogenic and abiogenic (Riding, 2011). Furthermore, both numerical models (Grotzinger and Knoll, 1999) and abiotic physical analogs (Mcloughlin et al., 2008) demonstrate that under some conditions, the formation of microbialite-like structures does not necessitate biological activity. While scientific discoveries continue to push back the boundaries of the living world, the distinction is often nuanced between microbial and non-microbial carbonates, and the complex issue of biogenicity is ever-present in the study of microbialites on Earth and the search for them elsewhere (e.g., Awramik and Grey, 2005; Rizzo et al., 2015; Gong et al., 2022). In practical terms, biogenicity consists in having an origin in the biosphere, i.e., having been alive or involved in the development of living organisms, and not only having been deposited at the same time and in the same place. Biogenicity studies attempt to determine the preservation processes of microbial mats as microbialites, which is particularly important in the search for early life in Precambrian rock successions. Whether for ancient structures preserved in deep-time geological formations, or for modern structures described

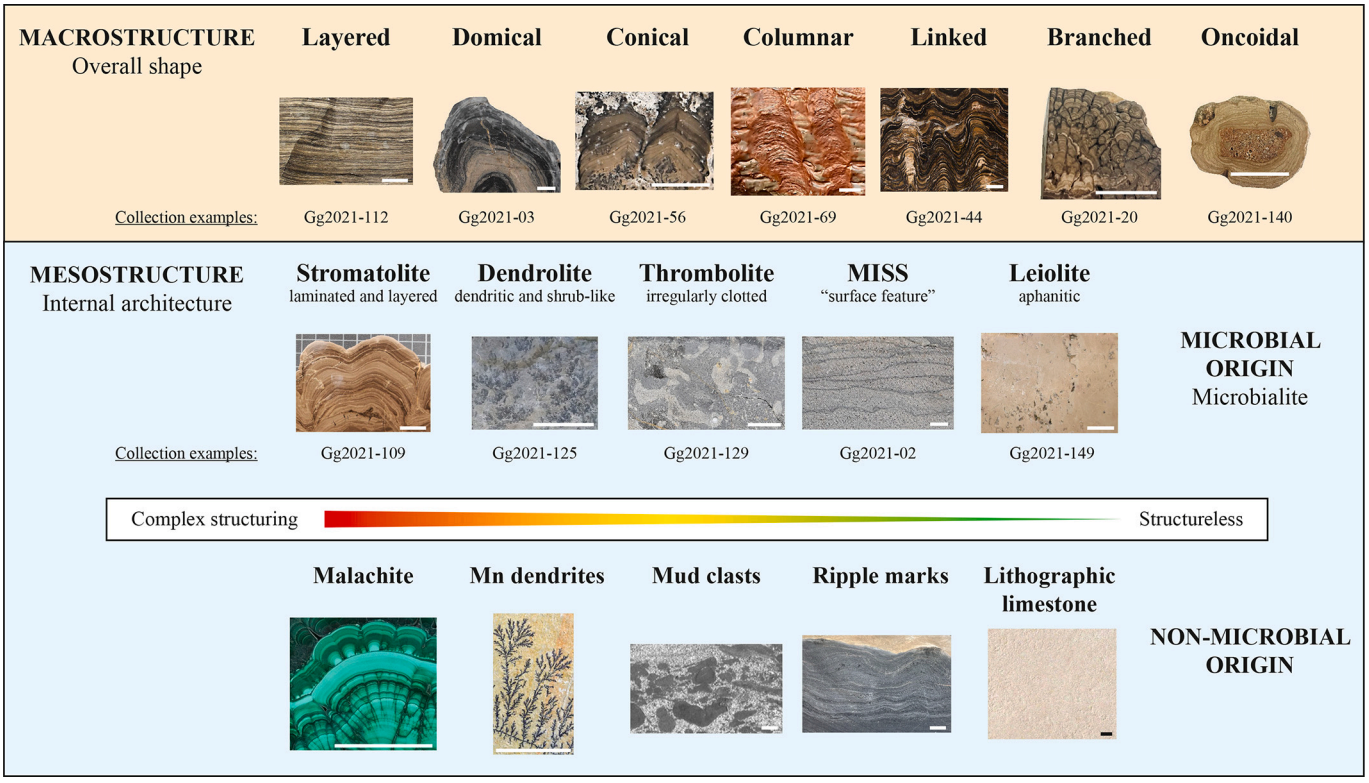

Fig. 1. Classification of microbialites by macrostructure and mesostructure (internal architecture) compared to similar structures of non-microbial origin. Photographs of microbialites come from the MNHN Microbialite Collection; "GgX-Y" is the museum inventory number. Photographs of mineral and rock structures of non-microbial origin also come from various MNHN collections. Scale bars are 2 cm.

in diverse environments where carbonate precipitation does not necessarily require metabolic activity, the biogenicity of microbialites is continually debated (García Ruiz et al., 2002; Schopf and Kudryavtsev, 2012; Allwood et al., 2018).

1.2. Microbialites through geological time: archives of the past

In addition to this exceptionally broad environmental distribution, the geological record of microbialites spans >3.5 billion years (Ga) of life history. In contrast to other marine chemical sediments, such as banded iron formations (BIF) that were deposited in anoxic marine environments almost exclusively prior to 1.8 Ga (Cloud, 1973), microbialites appear in all periods of geological time up to the present day. They often have a carbonate composition and are similar to non-microbial carbonates. They carry important mineralogical, geochemical, and isotopic information regarding Earth's chemical and biological evolution, especially in deep geological time (Riding et al., 2014; Sforna et al., 2014; Hohl and Viehmann, 2021; Wilmeth et al., 2022). Their abundance, form, and paleoenvironmental distribution have also evolved as the microbial biosphere itself responded to Earth system changes through time (Awramik et al., 1976; Knoll and Semikhatov, 1998; Hofmann, 2000; Riding, 2000). Thus, microbialites constitute an important reservoir of environmental and biological information, especially at the height of their abundance during the Archean and Proterozoic.

Theoretically, the Earth has been habitable since the first establishment of a hydrosphere by 4.3 Ga (Mojzsis et al., 2001; Wilde et al., 2001). Molecular clock analyses suggest an origin of phototrophy before 3.2 Ga and the divergence of the archaea as early as 4.11 Ga (Battistuzzi et al., 2004), implying even earlier ages for the last common ancestor of living organisms. One of the oldest purported pieces of evidence for life on Earth takes the form of putative stromatolites from the 3.7 Ga Isua Supracrustal Belt, Greenland (Nutman et al., 2016; Nutman et al., 2019; Nutman et al., 2021), however it remains to be seen as to whether these structures are truly of biological origin and not the product of structural deformation (Allwood et al., 2018; Zawaski et al., 2020). Two samples from this controversial locality are included in the collection and their data plotted alongside other Eoarchean-to-Paleoarchean microbialites in this study for comparative purposes only; we highlight that microbial influence during their deposition is highly uncertain at present. All other samples featured in this study have been rigorously screened to eliminate any for which a microbial origin may be dubious. The first sediments that are widely accepted by the scientific community as biological in origin date from the early Paleoarchean, with stromatolites and microbial mats preserved in the 3.48 Ga Dresser Formation (Pilbara craton, Australia; Van Kranendonk et al., 2008) and 3.47 Ga Hooggenoeg Formation (Kaapvaal craton, South Africa; Walsh, 1992; Hickman-Lewis et al., 2018). By 3.43 Ga, a remarkable stromatolitic reef system is preserved in the Strelley Pool chert (Pilbara craton, Australia; Walter et al., 1980; Sugitani et al., 2010), where several morphotypes are preserved on an ancient peritidal carbonate platform as a complex ecosystem with clear paleoenvironmental associations (Allwood et al., 2006).

Based on the reconstruction of Peters et al. (2017) for North American and Caribbean marine environments, the normalized occurrence of microbialites exhibits three major trends in their spatial and temporal distributions. First there is an increase from their first appearances in the Archean to the Early Paleoproterozoic (ca. 3800–2250 Ma). Then a period of dominance occurs from the Paleoproterozoic to the Meso-Neoproterozoic (ca. 2250–800 Ma) during which stromatolites are found in almost all marine carbonate units, and evolve from cm- to m-scale deposits to increasingly thick, multimetric platforms. New types of organisms contribute to the formation of microbialites in deeper environments, leading to a diversification of observed mesostructure, such as the generalized spread of thrombolites and the appearance and proliferation of dendrolites (Shapiro, 2007). The macrostructure of stromatolites also becomes more complex, sometimes showing multiple branching, and being able to form large columns or cones by vertical growth (Awramik and Sprinkle, 1999). Finally, from the end of the Neoproterozoic (ca. 700–541 Ma), a decline in records begins to lead to a very low average prevalence during the Phanerozoic (ca. 541–0 Ma), punctuated by a few resurgences, notably the one between the Cambrian and the Early Ordovician (ca. 482–511; Riding, 1992; Webby, 2002). Overall, structures are becoming more complex, but diminish in frequency, size, and diversity. Thus, from a biogeographic perspective, stromatolites are far more abundant in ancient environments, prior to the evolution and diversification of metazoans, which trigger predation, competition, and substrate modification (Monty, 1974; Awramik, 1992; Riding, 2006). Although in the modern ocean they are restricted to ecological niches where animal activity is limited, this is not necessarily the main reason for their decline. Stromatolite resurgences during the Phanerozoic do not entirely coincide with mass extinctions, and even today there are environments rich in diverse microbial and metazoan communities (e.g., Lake Tanganyika in Africa see Cohen et al., 1997; see also Rishworth et al., 2016 for a review) in which complex inter-growth tends to develop.

While the Earth has experienced multiple environmental upheavals, whether from a climatic, redox, or biological point of view, or by large oxygenation events, microbialites have thrived through these disturbances, and may record them (Hohl and Viehmann, 2021). Indeed, the ability of microbialites to thrive under extreme environmental conditions makes them unique archives for studying major environmental perturbations, often associated with mass extinctions, such as oxygenation/deoxygenation events. Archean shallow marine and freshwater carbonates support the hypothesis of oxygenic photosynthesis prior to the ca. 2.45 to 2.2 Ga “Great Oxidation Event” (GOE; see Lyons et al., 2014 for a review) by their role in the establishment of Archean “oxygen oases” (Anbar et al., 2007). Indeed, oxidation of small water bodies and surface environments likely occurred prior to oxygenation of the atmosphere or marine by the activity of benthic, mat-forming cyanobacteria (Lalonde and Konhauser, 2015; Sumner et al., 2015). During the “Boring Billion”, i.e., from ca. 1.85 Ga to 0.85 Ga (Holland, 2006), stagnant atmospheric O_2 levels and more oxidized surface ocean waters provide favorable conditions for microbialites. They thus remain a major feature of carbonate systems throughout much of the Proterozoic. Afterwards, despite a significant decline, they re-appear in many Phanerozoic carbonate producing systems that are subject to important redox, salinity, and/or nutrient perturbations occurring during continent-scale marine transgressive-regressive cycles (Bertrand-Sarfati and Monty, 2012; Peters et al., 2017).

1.3. Microbialites and their paleoproxy potential

Microbialites are often (but not universally) composed of chemical sediments; while these may include Fe- and Mn-oxides (e.g., Planavsky et al., 2009; Salama et al., 2013; Polgári and Gyollai, 2022), halite (e.g., Pope et al., 2000; Brigmon et al., 2008), gypsum (e.g., Petrash et al., 2010; Allwood et al., 2013), and phosphate (e.g., Bertrand-Sarfati et al., 1997; Morais et al., 2021), they are most often composed of different polymorphs of calcium carbonate minerals (i.e., aragonite, calcite) or Mg-rich carbonate minerals (e.g., magnesite, dolomite, ankerite) due to photosynthesis-driven alkalinization of their (micro-)environment and attendant increase in the saturation state of carbonate minerals (Aloisi, 2008; Zeyen et al., 2021). Many of the chemical sediments composing microbialites have long been recognized for their paleoproxy potential as they may retain elemental and isotopic signatures of the aqueous environments in which they precipitated (for reviews see Calvert and Pedersen, 2007; Robbins et al., 2016; Lau and Hardisty, 2022). Below we introduce some of the paleoproxies that are particularly relevant for carbonate microbialites and that we have analyzed using the MNHN Microbialite Collection to better understand the paleoproxy potential of microbialites relative to their non-microbialitic carbonate counterparts.

1.3.1. Carbon and oxygen stable isotope ratios in carbonate microbialites

Variations in the $^{13}C/^{12}C$ ratio as well as $^{18}O/^{16}O$ ratio due to isotopic fractionation are recorded during the precipitation of sedimentary carbonates and have proven to be important tools for exploring paleoenvironmental conditions, the carbon cycle, and aqueous geochemistry in carbonate-producing sedimentary environments throughout geological time.

The evolution of $\delta^{13}C_{carb}$ in deep geologic time is classically interpreted in the "carbon lever" framework (Holland, 1984). In this model, carbon is ultimately supplied to the Earth's surface via the degassing of CO_2 from the solid earth by metamorphism and volcanism. Carbon is then cycled through the ocean-atmosphere system, and ultimately exists by burial and subduction of organic matter and carbonate (see review by Berner, 1999). As the mean isotopic composition of volcanic CO_2 sources (estimated at −5‰; Cartigny, 2005) as well as organic matter ($\delta^{13}C_{org}$; estimated at −25‰; Havig et al., 2017 and references therein) are not thought to vary appreciably over geological timescales, the $\delta^{13}C_{carb}$ value is determined by the relative magnitudes of burial of organic carbon (i.e., the fraction of carbon buried as organic matter, F_{org}, whose value today is estimated at ca. 0.2) and carbonate carbon (i.e., the residual carbon exit flux, F_{carb}, whose value today is estimated at ca. 0.8). Over long geological timescales, this cycle is balanced, with the large majority of atmospheric and oceanic CO_2 sequestration occurring in carbonate sediments. In the absence of biological activity, carbonates are expected to have values approaching that of the mantle at ca. -5 ‰. In order to maintain $\delta^{13}C_{carb}$ values near zero, the carbon lever framework necessitates a relatively static ratio for the importance of organic versus inorganic carbon burial over geological time. However, this runs contrary to evidence that organic carbon burial rates have varied substantially over geological time (Hayes et al., 1999; Husson and Peters, 2017; Kipp et al., 2021). Furthermore, the magnitude of the organic carbon fluxes implied by some of Earth's largest carbon isotope excursions are difficult to explain (e.g., Bristow and Kennedy, 2008). This long-standing problem in the interpretation of ancient carbon cycling merits mention here but is beyond the scope of this study. Finally, it is important to note that carbon isotopes in carbonates do not always reflect global carbon cycle, but rather may reflect local dissolve carbone inorganic reservoir influenced by biogeochemical processes such as methanogenesis, methanotrophy, or Rayleigh distillation.

$\delta^{18}O_{carb}$ compositions of sedimentary carbonates can provide insights into paleotemperatures, aqueous geochemistry, and the relative importance of marine versus meteoric water sources in carbonate depositional environments (Ditchfield and Marshall, 1989; Jenkyns et al., 1994). It has long been noted that $\delta^{18}O_{carb}$ values in Precambrian carbonates show values that are significantly lower (lighter) than today (Degens and Epstein, 1962; Weber, 1965). The important secular evolution of $\delta^{18}O_{carb}$ over deep geological time has been classically interpreted as reflecting diagenetic processes, such as meteoric diagenesis, or interaction with high-temperature fluids during later metamorphism, both of which tend to generate lighter secondary $\delta^{18}O$ isotopic values in ancient carbonate rocks (e.g., Kaufman and Knoll, 1995; Melezhik and Fallick, 2003; see Knauth and Kennedy, 2009, for a succinct review).

Three non-mutually-exclusive hypotheses have been suggested to explain the trend towards significantly lower $\delta^{18}O_{carb}$ values in deep time. The first evokes higher paleotemperatures in ancient seawater, as carbonates precipitated at elevated temperatures are depleted in ^{18}O (Epstein et al., 1951). The application of typical carbonate paleothermometers indicate seawater temperatures of up to 100 °C during the Archean based on such low $\delta^{18}O_{carb}$ (see review by Jaffrés et al., 2007). This assumes that primary isotopic compositions are preserved in ancient carbonates. However, this leads to the second hypothesis that alteration by meteoric and diagenetic fluids has systematically shifted the oxygen isotopic composition of ancient carbonates towards lighter values. Indeed, the high porosity of carbonates makes them equally important archives of post-depositional fluid alteration (Tan et al., 2018), and this applies microbialites as well, where alteration and loss of fluid-mobile elements is also directly tied to porosity (Viehmann et al., 2023). The alteration hypothesis is often supported by additional proxy data for fluid-rock interaction (e.g., elevated manganese to strontium ratio), although this may be problematic for Precambrian carbonates deposited from seawater of dramatically different composition from today (see below, section 3.2).

Finally, it is possible that the oxygen isotopic composition of seawater evolved through geological time. The idea of secular evolution in the $\delta^{18}O$ value of global seawater faces a significant challenge in that oxygen isotope exchange with basalt during hydrothermal circulation acts to buffer $\delta^{18}O$ values of the global ocean to near zero over geological timescales (Muehlenbachs and Clayton, 1976). More recently, it was suggested that seawater-rock interaction may have been less efficient in deep geological time (Kasting et al., 2006) due to a higher heat flux and more important temperature gradient in the crust, such that the boiling and upwelling of water at shallower depths limited the efficiency of isotopic exchange during water-rock interaction. Indeed, recent studies examining the oxygen isotope compositions of sulfate (Killingsworth et al., 2019) and iron-oxides (Galili et al., 2019) both indicate that seawater may have been isotopically lighter by ca. 10 ‰ relative to today. If this last hypothesis proves correct, the light $\delta^{18}O$ values of carbonates, like those of ancient cherts (c.f. Knauth, 2005), cannot be considered exclusively as evidence of alteration by post-depositional fluids.

1.3.2. Rare earth elements in carbonate microbialites

Rare Earth Elements (REE) are powerful tracers of sedimentary provenance as well as specific aqueous conditions that generate fractionation between different REE in solution, which are in turn expressed as water column REE anomalies that may be preserved in chemical sediments such as carbonates (see reviews by Bolhar et al., 2004, and Tostevin et al., 2016), including carbonate microbialites (Webb and Kamber, 2000; Kamber et al., 2014). REE have short residence times in aqueous environments (e.g., ranging from ca. 50 yr for Ce to ca. 3000 yr for Lu; Nozaki, 2001) and are thus local paleoenvironmental tracers that have shown significant utility for reconstructing depositional environments based on their enrichments or depletions in ancient chemical sediments, such as freshwater versus marine environments (Bolhar and Van Kranendonk, 2007), the local importance of continental solute fluxes (Alexander et al., 2008), and the local redox environment (Bau and Dulski, 1996a). Furthermore, REE signatures can be highly distinctive and are generally unaffected by carbonate diagenesis (e.g., Hood et al., 2018; Liu et al., 2019) or high-temperature metamorphism (e.g., Bau, 1993; Cherniak, 1998; Bolhar et al., 2004). Yttrium (Y), while not a lanthanide, behaves similarly to holmium (Ho) but with slightly lower particulate reactivity in seawater, and supra-chondritic Y/Ho ratios are a useful indicator of open-ocean conditions (Byrne and Lee, 1993; Bau et al., 1995). Accordingly, Y is often presented alongside REE data (sometimes denoted REE + Y or REY; for simplicity we employ the term REE in this work for REE data that includes Y). Upon normalization of REE concentration data to a suitable reference material, such as chondrite or the upper continental crust (most often represented by the Post-Archean Australian Shale composite dataset, PAAS; normalization values for this work are from Taylor and McLennan, 1985), one can immediately visualize REE fractionation relative crustal REE sources.

Carbonate microbialites features generally appear to record the REE of the waters in which they formed (Webb and Kamber, 2000). While continental waters can have highly variable REE features, seawater of the open ocean presents a characteristic REE pattern typical that has remained broadly similar (with a few important exceptions) since 3.7 Ga (e.g., Bolhar et al., 2005). Open ocean seawater shows heavy REE (HREE) enrichment relative to light REE (LREE) as a consequence of the increasingly strong complexation with marine carbonate ions with progressively smaller lanthanide radii (Byrne and Kim, 1990; Zhong and Mucci, 1995). The particulate surface complexes of Y in seawater are less stable than those of REE of similar ionic radii such as Ho (Byrne and

Lee, 1993; Bau et al., 1995), making the Y/Ho ratio an important seawater signature that develops in natural waters with increasing salinity (Lawrence and Kamber, 2006), producing seawater-like Y/Ho ratios at salinities as low as 5–10 ppt (Tepe and Bau, 2016). Open seawater reaches Y/Ho ratios of 60 to 90 g/g in the modern ocean (Nozaki et al., 1997; compare to the PAAS Y/Ho ratio of 27; Taylor and McLennan, 1985). Finally, positive anomalies in both Gd and La represent another important and widely-applied seawater signature. Both show natural anomalies due to a combination of enhanced carbonate complexation relative to their neighbors (e.g., Kim et al., 1991) and differential fractionation during flocculation of REE with organic matter across salinity gradients though an estuary (e.g., Byrne and Kim, 1990). Note that the small natural Gd anomalies introduced here are different than the large anthropogenic anomalies in natural waters arising from the medical use of Gd contrasting agents (Bau and Dulski, 1996b). Considering the small magnitude of Gd anomalies in natural waters free of anthropogenic influence compared to that of La, Gd anomalies are not treated further in this manuscript.

Finally, two REE signatures with important paleoenvironmental applications may also be present in seawater and associated precipitates. PAAS-normalized cerium anomalies are of particular interest for paleoenvironmental reconstruction as they are generated by oxidation of Ce (III) to more immobile Ce(IV) as a function of the redox conditions of the original sediment source, those experienced during sedimentary transport, and those of the depositional environment. Important negative Ce anomalies become widespread starting in the Paleoproterozoic due to increasingly important oxidative Ce removal from seawater associated with upper water column oxygenation in the wake of the GOE (Warchola et al., 2018; Hodgskiss et al., 2021). Under redox-stratified water column conditions, oxidized cerium trapped in the sediment can be remobilized and released into anoxic bottom waters, driving the local development of positive cerium anomalies (e.g., Planavsky et al., 2009). Europium is another REE that shows redox-sensitive speciation under conditions relevant to Earth's surface. Positive Eu anomalies in natural water and their precipitates represent contributions from high temperature (>250 °C) reducing fluids, where Eu(III) is reduced to the more soluble Eu(II) form (Bau, 1991). Cooling of hydrothermal fluids, whether by conduction or mixing with lower-temperature fluids, results in the reoxidation of dissolved Eu(II) to Eu(III) and the loss of positive water column Eu anomalies (Bau et al., 2010). Marine chemical sediments of Archean age, whether banded iron formations, cherts, or carbonates (including carbonate microbialites), often show important positive Eu/Eu* anomalies due to the greater influence of high-temperature hydrothermalism on diverse aquatic habits of the early Earth (e.g., Bau and Dulski, 1996a, 1996b; Bolhar et al., 2004; Allwood et al., 2010; Kamber et al., 2014; Viehmann et al., 2015).

1.3.3. Redox-sensitive elements in carbonate microbialites

Enrichments of redox-sensitive elements such as iron (Fe), manganese (Mn), uranium (U), molybdenum (Mo), and vanadium (V) in carbonate chemical sediments are powerful tracers of Earth surface redox conditions. These elements demonstrate redox-dependent solubility as the result of valence changes as well as redox-sensitive ligand coordination that varies as a function of the amount of oxygen present in both continental and marine environments (e.g., Calvert and Pedersen, 1993; Russell and Morford, 2001; Wille et al., 2013; see Robbins et al., 2016 for review). In the case of the major elements Fe and Mn, both are solubilized under anoxic conditions, and form insoluble oxide precipitates in contact with free oxygen; Fe oxidizes rapidly and near-quantitatively at pH values greater than ca. 5 and at low O_2 partial pressures, while Mn oxidation is kinetically inhibited at all but alkaline pH conditions, and the Mn(II)/Mn(IV) couple has a higher oxidizing potential and requires higher O_2 partial pressures to drive oxidation and oxide precipitation (see Davison, 1993, for review). These metals are thus present in higher abundances in natural waters under low-O_2 conditions and removed as oxides with different degrees of efficiency with increasing redox potential.

The trace elements U, Mo, and V act somewhat inversely to Fe and Mn; all three are solubilized from oxic terrestrial weathering environments and require oxic to suboxic conditions to remain in solution; under anoxic water-column conditions, they are preferentially scavenged into sediments. Accordingly, in an O_2-depleted ocean-atmosphere system, sedimentary enrichments of these trace elements are minimal, whereas anoxic sediments in contact with an O_2-rich ocean-atmosphere system show enrichments that scale with atmospheric or marine oxygenation. Indeed, the enrichment of these redox-sensitive elements as well as their stable isotope compositions in ancient marine sedimentary rocks has been widely used to constrain the chronology of oxygenation on Earth (e.g., Arnold et al., 2004; Anbar et al., 2007; Wille et al., 2007; Sahoo et al., 2012). There exist subtle but important differences in the redox-driven behavior of these trace elements. Today, oxidative continental weathering results in the release of U(VI) from U (IV)-bearing uraninites (Grandstaff, 1976) and supplies most of the uranium entering the ocean via rivers (Dunk et al., 2002), where it ultimately exits by sequestration largely in anoxic sediments (Anderson et al., 1989). U(VI) is easily integrated into the calcite lattice due to its small size (Sturchio et al., 1998) and is enriched in carbonates precipitated under oxic conditions. Vanadium is similarly supplied by continental weathering in the form of the oxyanion vanadate and is sequestered similarly to uranium and molybdenum into reducing sediments deposited under anoxic conditions (Breit and Wanty, 1991). Molybdenum is supplied by oxidative continental weathering of sulfide minerals, and to a lesser degree marine hydrothermalism, and is largely sequestered by organic rich sediments deposited under anoxic conditions (McManus et al., 2002), with the added particularity that its removal is significantly enhanced via thiolation in the presence of aqueous S(-II) (Helz et al., 1996, 2011; Vorlicek et al., 2004). Carbonate sediments may capture all these different processes by the enrichment or depletion of these two "O_2-immobile" major elements and three "O_2-mobile" trace elements. In this study we evaluate the systematics of these redox-sensitive elements in carbonate samples of the MNHN Microbialite Collection to evaluate whether they record the evolution of Earth's surface redox conditions in a manner similar to non-microbialitic carbonates.

1.4. The MNHN microbialite collection: a community resource for studying microbe-sediment interactions through time

Microbialites are inherently diverse, distributed worldwide and increasingly protected – all factors that complicate their systematic and comparative study. To address these issues and promote microbialite research in general, we have assembled a large collection of microbialite samples accessible for examination by the public as well as for study and sampling by academic researchers. This collection was initiated on behalf of the MNHN, in accordance with its mission to promote research, specimen conservation, teaching, and public outreach. It is stored in the historical reserves of the MNHN in Paris (Fig. 2). Here, several hundred thousand specimens of rocks, minerals, fossils, and archeological artefacts have been collected and curated since 1626, initially as a Royal collection (the "Droguier du Roi") that laid the foundation for one of the world's first natural history museums, formally taking on this title in 1793. The ultimate goal of the MNHN Microbialite Collection is to provide a comprehensive, curated, and accessible collection, along with associated metadata, including geochemical data, that would be available for the microbialite scientific community in perpetuity.

The MNHN Microbialite Collection is comprised of historical MNHN samples as well as new acquisitions secured from over 37 researchers to date (Supplementary Table 1), and is constantly growing. It includes numerous rare specimens, for example purported microbialites from the >3.7 Ga Isua Supracrustal Belt (West Greenland), from the 3.48 Ga Dresser Formation and 3.43 Ga Strelley Pool chert (Pilbara, Western Australia), and specimens of modern microbialites from the shallows of

Fig. 2. The historical collections of the MNHN. (A and B) Sample Gg2002–35, a stromatolite from Potosi, Bolivia, collected for the MNHN by Alcide d'Orbigny in 1834, i.e., before the definition of stromatolites. Its historic inventory number 169 is referred to in one of the contemporary catalogs (C) as "169 – Calcaire magnésien, concrétionné jaunâtre. Santa Lucia." (Translation: "magnesian limestone, yellowish and concretioned"). (D) Samples from the MNHN Microbialite Collection are packed in LAB boxes after the curation and sampling and stored in the drawers of the historical reserves of the Geology and Mineralogy Gallery of the MNHN.

Hamelin Pool (Shark Bay, Western Australia). In concrete terms, this collection gathers together samples from all continents (except Antarctica) and covers all of geological time since the first presumed traces of life on Earth.

Microbialites have long been of interest for understanding the co-evolution of the atmosphere, hydrosphere, and biosphere over geological time, as well as to trace and understand major perturbations in Earth's history. Such a large microbialite collection begs comparative study, whereby specific questions regarding microbialite archives may be addressed such as: are microbialites reliable recorders of the paleoenvironments in which they formed? Does the chemical and isotopic composition of microbialites trace the evolution of Earth's major biogeochemical cycles in the same way as their non-microbial carbonate counterparts? What are the compositional characteristics of microbialites deposited in different environments, and do they change through Earth history? To begin to address these questions, we provide here high-precision trace element data as well as carbonate C and O stable isotope data for over 400 samples out of the ca. 1370 that currently constitute the collection, and compare them to a large database of carbonates from literature in an attempt to understand the nature and fidelity of microbialites as chemical and isotopic recorders of Earth system change.

2. Methodology

2.1. Curation and Sampling

In total, for this study, we inventoried over 1370 specimens of microbialites, stored under 480 inventory numbers; multiple specimens from the same strata, locality and age are classified under the same inventory number. All samples are part of the General Geology Collection of the MNHN and thus possess inventory codes beginning with "Gg". The Microbialite Collection is comprised of a combination of samples that were already in the General Geology Collection, however a large number of samples were added in 2021 as the result of a concerted effort to establish this microbialite subcollection. Associated data were collated from historical catalogs when available, and for both historical and newly entered samples, efforts were made via literature search to establish depositional age constraints, state of preservation or metamorphic degree, and stratigraphic, depositional, and paleoenvironmental context. Samples were packed in crystal polystyrene LAB boxes (transparent, chemically neutral, and UV resistant, Fig. 2D), and were stored in a dedicated section of the General Geology Collection archives for easy access by researchers. Most samples of the Microbialite Collection are now included in the MNHN public database which can be consulted at https://science.mnhn.fr/institution/mnhn/collection/gg/item/search. All metadata, including geochemistry data, associated to the MNHN Microbialite Collection at the time of publication has been made available at EarthChem repository (Fogret et al., 2024); additional information on the collection is also available at https://www.microbialites.com/collection-and-database/.

For chemical and isotopic analyses, 478 microbialites were sampled from the collection using an electric hand drill equipped with tungsten carbide drill bits (HP-4 series, Karnasch GmbH, Heddesheim, DE). Between samples, the bit was cleaned with ethanol and dried with compressed air. The powders analyzed were extracted from the most representative mesostructures of the microbialite under consideration after its complete description. For this reason, some samples have been drilled in several spots, especially if from a macrostructure that reveals an evolution of the depositional environment (e.g., between the base and the top of a stromatolitic column), or if they present different mesostructures (e.g., stromatolitic and dendrolitic areas in the same sample). Between 30 and 200 mg of powder was recovered on new aluminum foil and directly transferred into 5 ml polypropylene vials for analysis and archiving. While targeted micro-drilling was performed, volumes approaching a cubic cm were sampled and homogenized into powder, such that we consider them bulk analyses; future work using in-situ methods (e.g., SIMS, LA-ICP-MS) would certainly reveal finer-scale variation and heterogeneity that we are admit are certainly present but not captured but our current study.

2.2. Stable carbon and oxygen isotopic analysis

Most of the stable carbon and oxygen isotope compositions ($n = 253$)

of the microbialite samples reported here were determined following the analytical procedure of Santrock et al. (1985) using a ThermoFisher Delta V Advantage isotope-ratio mass spectrometer (IRMS) located at the SSMIM (*Service de Spectrométrie de Masse Isotopique du Muséum*), the isotopic analysis platform of the MNHN. Another portion of the samples (n = 166) was measured on a MAT253 instrument of the *Pôle Spectrométrie Océan* (PSO; Plouzané, France) using identical procedures but without the use of the Marbre LM standard (see below). In both cases (n = 419 in total), the measurements were carried out on powdered samples (between 60 and 90 μg) which were weighed and then transferred in glass vials to be placed into a KIEL IV Carbonate Preparation Device. This instrument extract and purify $CO_{2\ gas}$ from carbonate ($CaCO_3$), in a thermostatic chamber at 75 °C for 8 min, by adding orthophosphoric acid (H_3PO_4) according to the following equation:

$$3CaCO_{3\ (s)} + 2H_3PO_{4\ (aq)} \rightarrow 3CO_{2\ (g)} + 3H_2O_{(g)} + Ca_3(PO_4)_{2\ (aq)}.$$

For each analytical run comprising 48 analyses, 10 standards were dispersed throughout the run to correct for shifts in mass bias and linearity and to calibrate the data, namely: NBS-19 (National Bureau of Standards, U.S.A.), MarbreLM (SSMIM internal standard, used for samples analyzed at the MNHN), and CAMIL-21 (in-house standard of Neoproterozoic cap carbonate available from P. Sansjofre). The percentage of carbonate in each sample was calculated using the mass 44 signal. All isotopic data are expressed in permil (‰) relative to V-PDB. The internal precision, as determined by replicate standard analyses, was better than 0.03 ‰ for $\delta^{13}C_{carb}$ and better than 0.06 ‰ for $\delta^{18}O_{carb}$ (2 standard errors; $2\sigma_x$). The external precision, as determined by the mean of the differences between replicate samples (n = 32), is better than 0.09 ‰ for $\delta^{13}C_{carb}$ and better than 0.13 ‰ for $\delta^{18}O_{carb}$ ($2\sigma_x$).

2.3. Major, trace, and rare earth element analyses

The concentrations of selected major, trace, and rare earth elements (REE) in carbonate samples were determined using an ElementXR high-resolution inductively coupled plasma mass spectrometer (HR-ICP-MS) of the PSO. Firstly, samples were weighed and digested in a class 1000 clean laboratory using a weak carbonate leach procedure to preferentially liberate elements from the carbonate without digesting any clays, oxides, or crystalline silicates that may have been present in the microbialites samples, following the method of Rongemaille et al. (2011). All concentrations are reported as leachable concentrations with respect to the total mass of the leached sample. After weighing the powdered samples (between 30 and 60 mg) in *Savillex* PFA vials, 1 ml of 5% trace-metal grade acetic acid (Fisher Scientific) was added, and the vials were vortexed by hand. Then, 100 μl of the leachate was pipetted from the top of the aqueous phase after the samples had settled overnight at room temperature; no centrifugation, decantation, or filtration was additionally employed. The small aliquot of leachate was added to 5 ml polycarbonate tubes and diluted with 4.9 ml of 2% PFA-distilled nitric acid (HNO_3) containing 2 ppb indium (In) as an internal standard. HR-ICP-MS analyses were performed using a cyclonic spray chamber with a PFA nebulizer and standard (H) cones. Samples were measured in low-, medium-, or high-resolution mode, depending on the potential interferences for each element and the sensitivity required. Data were corrected for instrumental drift using In measured in low, medium, and high-resolution mode and calibrated against commercial multi-element solutions prepared gravimetrically to concentrations of 50 ppb, 5 ppb, and 0.5 ppb. The 5 ppb standard was repeated every 10 samples to further correct instrumental drift and to calculate internal precision. Detection limits were determined by the average values of the 2% HNO_3 rinses that were passed and analyzed between each sample. External precision, as determined by replicate analysis of the CAL-S international standard (which was passed through the entire preparation process, i.e., weighing, leaching, and dilution, and included in every run) was better than 5% (one relative standard deviation, RSD) for REE and Y (Supplementary Fig. 1) and ca. 10% (1 RSD) for other trace elements. All presented REE spectra and anomaly indicators were shale-normalized to post-Archean Australian shale (PAAS) using the values of Taylor and McLennan (1985) with the exception of Y/Ho, Pr/Yb, and Sm/Yb (which are reported in g/g).

As discussed in the introduction, anomalies in specific REE may carry important information about microbialite depositional environments. Such anomalies may be evaluated quantitatively as the normalized ratio Ln/Ln*, where Ln* is the lanthanide concentration expected by extrapolation of an appropriate combination of close neighbors around the lanthanide Ln under consideration (Lawrence et al., 2006). Values below unity represent negative anomalies, and above unity, positive anomalies. Extrapolations for Ln* are often performed semi-logarithmically (i.e., using a geometric mean), resulting in straight-line extrapolations on semi-log-scale REE diagrams; calculation using geometric means provides for the most robust calculation of anomalies over typical REE compositional ranges such as that covered in this study (Barrat et al., 2023). In this work, europium (Eu/Eu*), lanthanum (La/La*), and cerium (Ce/Ce*) anomalies are calculated geometrically using the following equations:

$$Eu^* = Sm\ x\ (Sm/Nd)^{1/2} \quad (1)$$

$$La^* = Pr\ x\ (Pr/Nd)^2 \quad (2)$$

$$Ce^* = Pr\ x\ (Pr/Nd) \quad (3)$$

as per Lawrence et al. (2006), while other useful indicators, such as the Y/Ho and Pr/Yb (an anomaly-free indicator of light vs. heavy REE enrichment), are calculated on a g/g basis.

The instrument was tuned to minimize oxide production, which was further quantified by the analyses of control solutions (Ba—Ce, Pr—Nd) before each session. Despite low oxide production rates (measured BaO/Ba <0.0012%), samples with the highest Ba concentrations nonetheless generated false Eu anomalies by the interferences of $^{135}Ba^{16}O$ and $^{137}Ba^{16}O$ on masses corresponding to ^{151}Eu and ^{153}Eu, respectively, that were generally well-corrected by subtraction of BaO interferences (compare Supplementary Fig. 2A and B). Nonetheless, as a precaution, Eu/Eu* data were not plotted for 14 samples that had Ba/Sm ratios exceeding 1000 g/g.

3. Results and discussion

3.1. Situating the MNHN microbialite collection in time and space

The MNHN Microbialite Collection is intended to provide a community resource for the study and comparison of microbialites spread across geological time and from all over the globe. Excluding a few samples for which the age or location are not precisely known, >1340 samples of well-constrained provenance currently comprise the collection (Fogret et al., 2024). The temporal and modern spatial distribution of the samples constituting the MNHN Microbialite Collection are presented in Figs. 3 and 4. Despite the large number of samples, it can be seen in these figures that sampling bias affects these distributions. As for the distribution of the MNHN collection through geological time, certain eras are over-represented due to an uneven distribution of specific periods of more or less scientific interest. For example, despite their limited preservation, Archean samples are widely studied due to their important implications for early biospheric evolution, and this is reflected by their numbers in the MNHN collection. Conversely, an overabundance of modern samples, despite the scarcity of microbialites today relative to most of geological history, is explained by their readily preserved nature and the high scientific interest in the study of present-day stromatolites to understand ancient ones.

The geographical distribution similarly reflects biases in participation in the collaborative networks of researchers examining microbialite

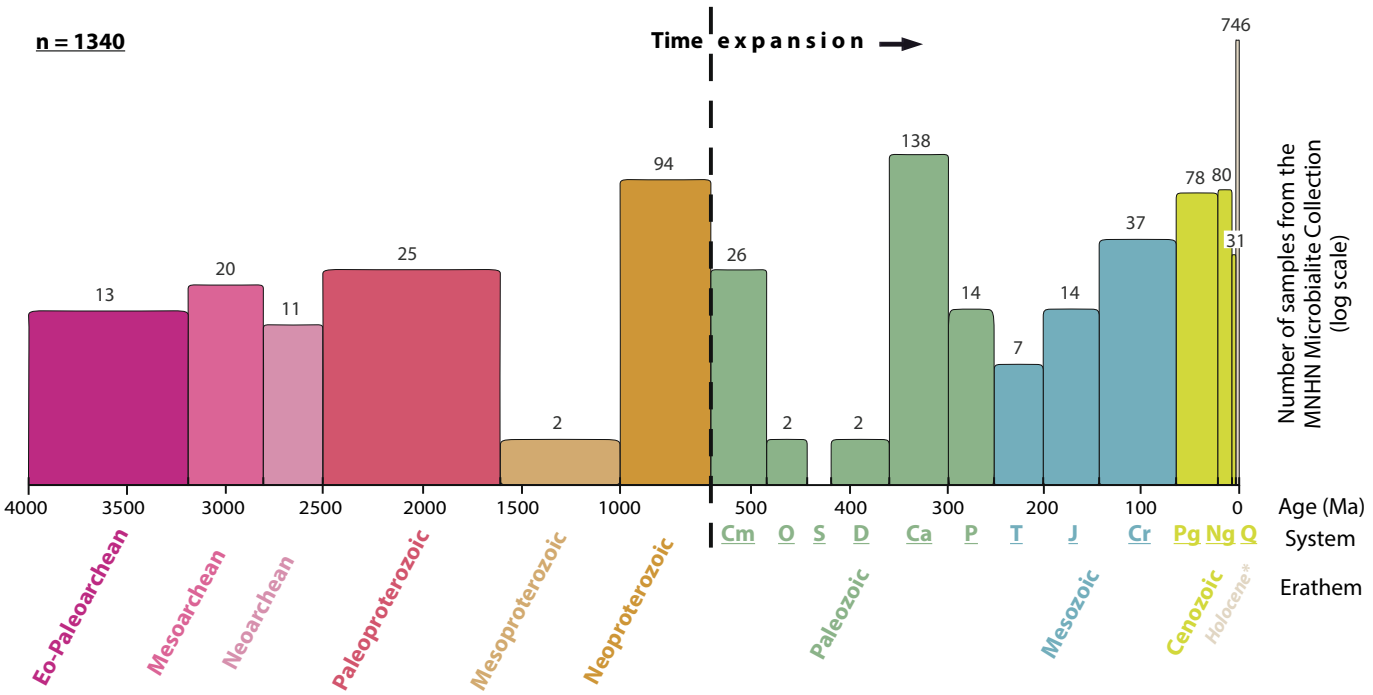

Fig. 3. Histogram of samples according to their age representing the 1340 samples currently assembled in the MNHN Microbialite Collection. Holocene samples are represented separately from the rest of the Cenozoic samples. Note the difference in timescales between the Phanerozoic and Precambrian.

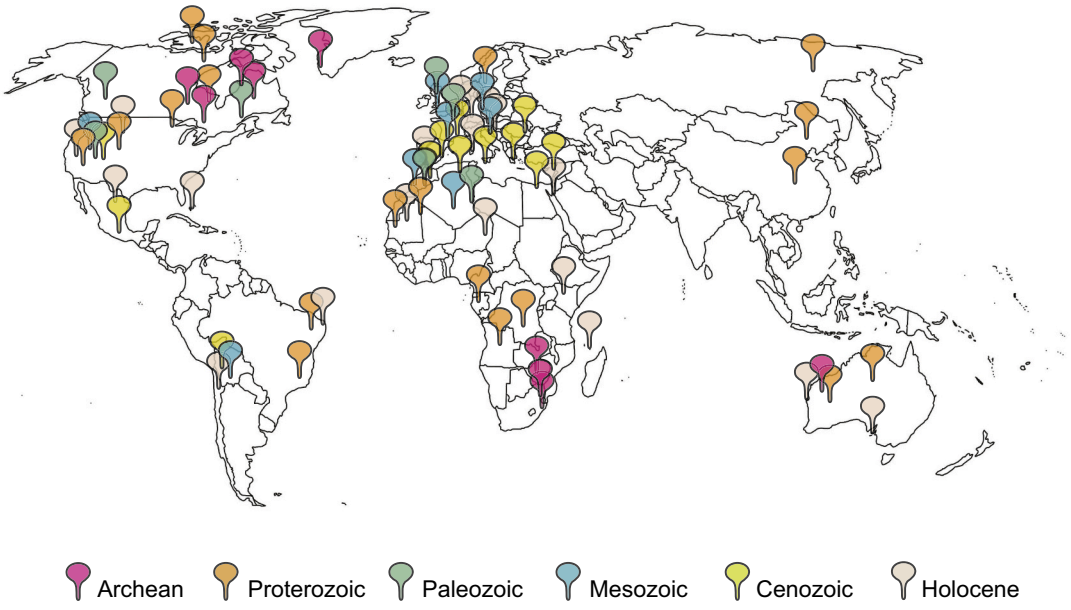

Fig. 4. Global map of the location of the 1340 samples comprising the MNHN Microbialite Collection at the time of print. Note that each individual sample is not shown on this map, but simply the locations and ages of the samples, for a clearer understanding.

records, as well as areas that are more or less difficult to access due to the nature of the individual field sites or even issues regarding regional stability and accessibility from a socio-political context. Currently, the MNHN Microbialite Collection spans all continents except Antarctica (Fig. 4) and favors samples largely from old provinces (e.g., North America, Amazonia, West Africa, Sahara, Congo, South Africa, Australia) but also from some areas with specific hydrological and biogeochemical conditions conducive to microbialite formation (e.g., Mediterranean coast, Mexican lakes, Australian gulf). Despite its limited sample size and thus predictive power, the MNHN collection shows certain trends in temporal distribution that have been previously observed in meta-analytical studies (see section 1.2). Notably, in the MNHN collection, microbialites spanning the Paleoproterozoic to Neoproterozoic are relatively abundant, and a decline in abundance is seen in the earliest Phanerozoic. Both observations were first noted by Awramik and Sprinkle (1999), supported by later work by Riding, 2000, Riding, 2006, Riding, 2011), as well as the more recent meta-analysis, for North America–Caribbean region, using machine reading tools (Peters et al., 2017). Thus, despite a sample size necessarily inferior to those available for larger meta-analytical studies, the MNHN collection appears broadly representative in its temporal distribution of microbialites relative to current understanding of their actual abundance evolution

over geological time. The degree to which the samples may be attributed to specific paleoenvironments is highly dependent on age; e.g., for Quaternary samples, the depositional environments are directly observable and highly nuanced classifications are possible (see section 3.3.3). For older Phanerozoic samples and especially for Precambrian samples, the attribution of highly specific paleoenvironments is subject to high uncertainty; for this reason, for most samples in the MNHN Microbialite Collection we avoid classification more specific than marine vs. non-marine unless highly robust independent paleoenvironmental constraints exist.

To evaluate how the MNHN Microbialite Collection, and carbonate microbialite geochemical records in general, record important patterns of Earth surface geochemical evolution, in the following sections we compare their stable carbon ($\delta^{13}C_{carb}$) and oxygen ($\delta^{18}O_{carb}$) isotope compositions, as well as paleoenvironmental and redox signatures for selected elements, against large geochemical data compilations representing carbonate rocks in general. We precede these interpretations by an evaluation of the reliability of the paleoproxies treated herein, detailed below.

3.2. Reliability of carbonate microbialite paleoproxies

While carbonate sediments may capture chemical and isotopic signatures from their depositional environment and thus form the basis of multiple geochemical paleoproxies, they are also susceptible to post-depositional modification as the result of dissolution and reprecipitation, recrystallization, and elemental and isotopic exchange with alteration fluids during diagenesis and metamorphism. Furthermore, detrital contamination, as well as the presence of specific mineral phases such as Fe- and Mn-oxide, phosphates, and sulfides, may all act to perturb paleoproxy signals that were originally developed for application to sediments dominated by highly pure carbonate minerals. Correspondingly, as a function of the chemical composition or alteration history of the carbonate sample in question, not all potential carbonate paleoproxy signals necessarily reflect depositional conditions. In this section we examine our dataset in light of potential secondary effects that may perturb the paleoproxy systems investigated in this study.

3.2.1. Mineralogical and alteration effects on carbonate proxies

Carbonate minerals are subject to a series of transformations that begin at sedimentation, proceed from early sedimentary diagenesis all the way through to peak metamorphism, and may continue upon surface exposure and supergene weathering (for reviews, see Fantle et al., 2010, 2020; Swart, 2015). From the first application of oxygen isotopes in carbonate minerals as a temperature paleo-proxy, Urey et al. (1951) recognized that alteration via solid-state diffusion meant that crystals smaller than 1 mm may not preserve their original isotopic compositions over long (million-year) timescales. Later workers realized that recrystallization, and not solid-state diffusion, was the primary process modifying the chemical and isotopic composition of modern carbonates during burial diagenesis (Gieskes et al., 1975; Sayles and Manheim, 1975), and that this process may affect both elemental (e.g., Mg/Ca; Baker et al., 1982) and isotopic ($\delta^{18}O$; Killingley, 1983) compositions. In some cases, recrystallization-driven early diagenetic elemental and isotopic redistribution may represent the dominant control over putative marine carbonate proxy signals (e.g., Jones et al., 2019), and caution is clearly warranted in their interpretation.

Carbonate recrystallization during diagenesis and metamorphism can be traced using elemental ratios. In general, elements with ionic radii larger than Ca (e.g., Sr) tend to be preferentially incorporated into more disordered carbonate minerals (e.g., aragonite) whereas those with radii smaller than Ca (e.g., Fe, Mn) are preferentially substituted into more ordered carbonates such as calcite and dolomite (Veizer, 1983). The net result is increasing Mn/Sr and decreasing Sr/Ca during carbonate recrystallization. The ensemble of non-REE based proxies (REE proxies discussed separately below, section 3.2.2) examined in this study are plotted against Mn/Sr and Sr/Ca in Supplementary Figs. 3 and 4, respectively. Carbonate carbon and oxygen isotope compositions generally tend towards lighter values, and U and Mo concentrations decrease, with increasing Mn/Sr, while Mn and Fe increase (Supplementary Fig. 3); the opposite is observed for Sr/Ca (Supplementary Fig. 4). No systematic variation with either indicator is observed for vanadium concentrations. Importantly, in the Supplementary Figs. 3 and 4 where the data are color-coded according to age, it is clear that older samples occupy the high Mn/Sr – low Sr/Ca space, and samples tend to lower Mn/Sr and higher Sr/Ca with age. Conventionally, these trends could be taken to indicate that in the MNHN carbonate microbialite dataset, lighter stable isotope compositions, depressed U and Mo concentrations, and elevated Mn and Fe concentrations are all a consequence of important recrystallization-driven post-depositional modification of the most ancient samples, and that younger samples were less affected. However, this interpretation is clearly non-unique when applied to carbonates spanning such a large period of Earth history. Specifically, it is at odds with independent evidence for seawater in deep geological time that as significantly lighter with respect to oxygen isotopes (Galili et al., 2019; Killingsworth et al., 2019), more ferruginous (e.g., Holland, 1973) and manganiferous (e.g., Robbins et al., 2023), and significantly depleted in U (Partin et al., 2013a, 2013b) and Mo (reviewed by Thoby et al., 2019) relative to modern seawater. Furthermore, partitioning of U and Mo should be enhanced, and not depressed, with recrystallization to more ordered carbonate minerals, whereas the MNHN carbonate microbialite data show the opposite trend. The most parsimonious explanation for the above is that the evolving major, trace, and isotopic composition of seawater has played a primary role in setting these signatures. As a corollary, while they are certainly useful when examining carbonates that are all of contemporaneous age, alteration indicators such as Mn/Sr and Sr/Ca ratios may be of limited utility when comparing carbonate sediments deposited over such large swaths of Earth history and that formed under correspondingly diverse chemical and redox conditions. Nonetheless, despite the long-recognized difficulty in distinguishing true paleoenvironmental signals from secondary overprints in ancient and altered carbonate rocks, as seen below in sections 3.3 to 3.5, the carbonate microbialite record examined here is remarkably consistent with multiple independent lines of evidence describing the long-term chemical evolution of the Earth system.

3.2.2. Isolating the carbonate signal: influence of carbonate impurities on REE signatures

Many carbonate paleoproxies are based on the partitioning behavior of elements or isotopes into pure carbonate minerals. However, natural carbonate-rich sediments are never pure, but rather contain a variety of secondary mineral phases that may also contain analytes of interest. Partitioning of elements into chemically pure carbonate results in only weak enrichments, and by consequence, even trace amounts of secondary mineral phases may dominate elemental budgets at the whole-rock level. For example, chemically pure carbonates often contain trace elements such as REE at concentrations that are 50 to 1000 lower than the average continental crust (e.g., Webb and Kamber, 2000). For this reason, and as was done for this study, elemental proxies in carbonate sediments are often analyzed using weak leach approaches that chemically target the pure carbonate fraction while avoiding the dissolution of secondary mineral phases. These include detrital materials such as clays, metal sulfides or oxyhydroxides such as Fe- and Mn-oxides, and phosphates. Below we examine our REE dataset with particular regard to potential biases that might arise from elemental contribution from secondary phases despite the use of a weak-leach digestion approach.

As mentioned above, the differential partitioning of cations into different carbonate minerals means that carbonate mineralogy may exert control over carbonate elemental enrichment; this clearly seen in the MNHN carbonate microbialite data in the case of carbonate-

leachable Fe contents when examined against sample Mg/Ca ratios (Supplementary Fig. 5A); as mentioned in section 3.2.1, partitioning of elements with ionic radii smaller than Ca, such as Fe and REE, should be favored into more crystalline, high Mg/Ca carbonate minerals such as ankerite and dolomite (Fantle et al., 2010). Surprisingly, contrary to the above example for Fe, no clear scaling relationships between total REE contents and Mg/Ca (positive relation expected) nor Sr/Ca ratios (negative relation expected) are observed (Supplementary Fig. 5B and C); we speculate that this may relate to the lower concentrations of REE compared to Fe in most diagenetic or metamorphic waters, and the greater immobility of REE more generally. The presence of REE-rich authigenic mineral carrier phases such as sedimentary phosphates and Fe- and Mn-oxides can significantly modify whole-rock REE signatures, however in the MNHN carbonate microbialite dataset, no trends exist between the REE anomaly indicators Eu/Eu*, La/La*, Ce/Ce*, and Y/Ho, and the leachable concentrations of P (Supplementary Fig. 6), Fe (Supplementary Fig. 7), or Mn (Supplementary Fig. 8). Furthermore, the slopes of REE spectra (as evaluated by the Pr/Yb mass ratio) show no relation with P, Fe, nor Mn concentrations, and significant middle REE enrichment that is characteristic of phosphate-associated REE is also absent across two orders of magnitude of leachable P contents (as evaluated by the Sm/Yb mass ratio; Supplementary Fig. 6F). Together, these data indicate that the potential presence of phosphates and Fe-Mn-oxides did not make significant contributions to the REE spectra presented here and confirms the suitability of the weak leach method of Rongemaille et al. (2011) employed herein that was specifically

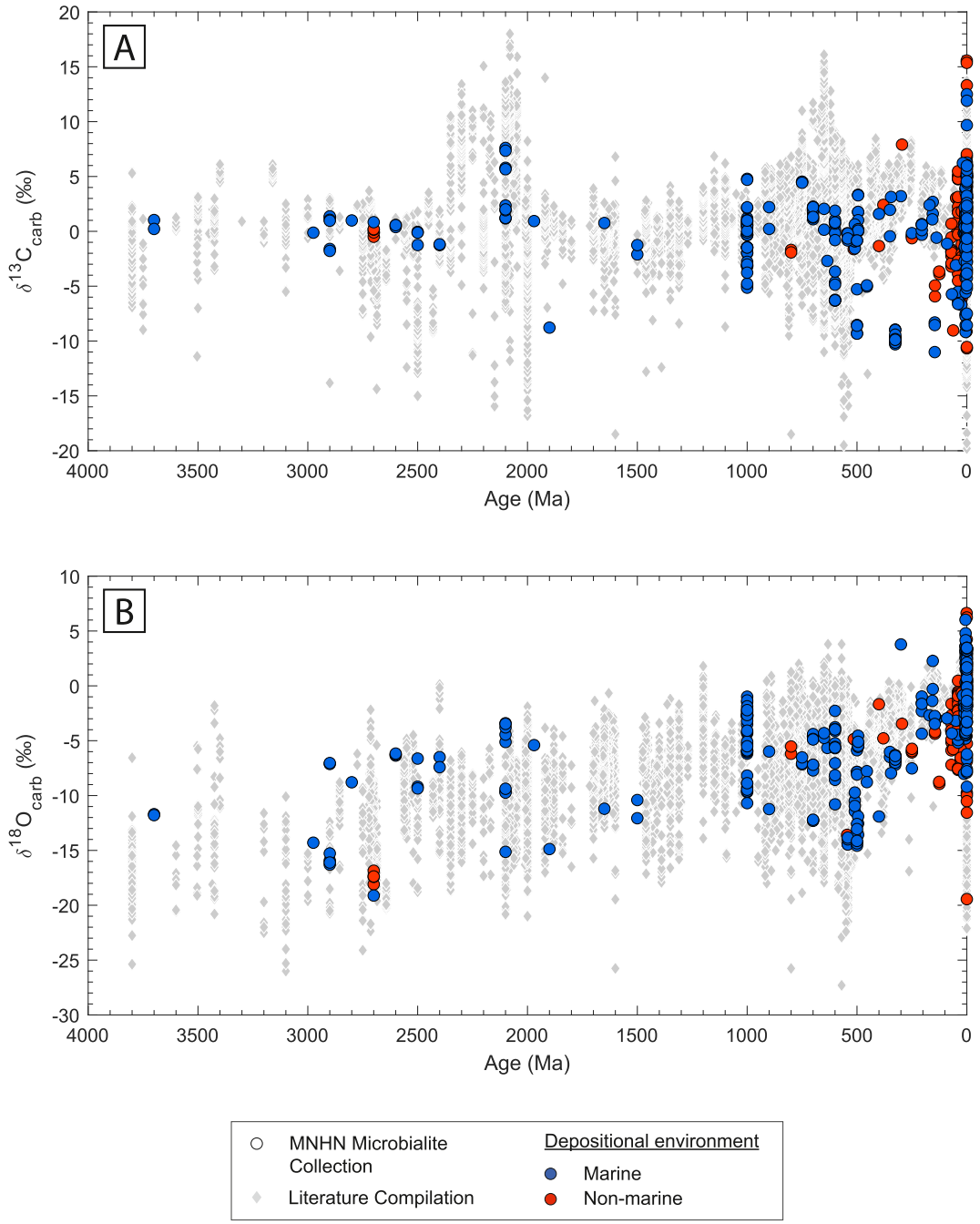

Fig. 5. Evolution of $\delta^{13}C_{carb}$ (A) and $\delta^{18}O_{carb}$ (B) in microbialites and marine carbonates over geological time. Each scatter plot is composed of 392 data points from samples analyzed in the MNHN Microbialite Collection (colored circles) and 24,467 data points compiled from literature (grey diamonds, compilation by Havig et al., 2017).

designed to minimize digestion of these phases.

Detrital contamination is especially problematic for REE- and redox-sensitive carbonate elemental paleoproxies as the concentrations of the elements in question tend to be hundreds to thousands of times higher in detrital materials such as clays and weathering-resistant accessory minerals. Indeed, Supplementary Fig. 9 reveals positive scaling between leachable total REE and Al concentrations that spans nearly three orders of magnitude in Al concentrations. Despite the strong general correlation, REE anomaly indicators such as Eu/Eu*, La/La*, Ce/Ce*, and Y/Ho, as well as the REE slope indicator Pr/Yb, show no systematic variation with Al concentrations. Rather, the vast majority of samples show leachable Al contents that are two orders of magnitude below continental crust values, and important REE anomalies persist up to the highest leachable Al contents determined in this study (approaching 0.7 wt% Al). Simple mixing models reveal that detrital contamination had little effect on REE systematics (Supplementary Fig. 9), consistent with the weak leach technique employed (5% acetic acid), and accordingly, no samples were excluded from consideration on the basis of Al concentrations. The clear positive correlation between total REE concentrations and Al concentrations noted above, but without apparent effects on REE anomaly indicators at all but the highest Al concentrations, is often observed in large chemical sedimentary datasets and may have multiple origins beyond simple mixing of detrital material. For example, if chemical sediments accumulate both water column-derived REE and Al-rich detrital material simultaneously as a function of time, a correlation between total REE and Al concentrations would be expected without Al-rich detrital material necessarily dominating the whole-rock REE budget. Regardless, for the REE data presented in this study, it can be affirmed that carbonate impurities, whether in the form of detrital materials, phosphate minerals, or Fe- and Mn-oxides, had little role on the REE proxy indicators in the MNHN carbonate microbialites examined in this study.

3.3. Microbialites as recorders of the evolution of Earth's carbon cycle and hydrosphere

The $\delta^{13}C_{carb}$ and $\delta^{18}O_{carb}$ values determined in this study from the MNHN Microbialite Collection are tabulated in Fogret et al. (2024) and plotted in the Fig. 5. The mean and median $\delta^{13}C_{carb}$ values across all samples are −0.21 ‰ and + 0.38 ‰, respectively. Carbon isotope variability is greatest among Holocene samples, which span a large diversity of modern environments and accordingly cover a wide range of values (2σ = 8.99 ‰, mean = +2.03 ‰, median = +2.28 ‰). On the contrary, Archean samples show a very narrow range of carbon isotope compositions (spanning only 3.15 ‰ in total) and are centered around a mean value of $\delta^{13}C_{carb}$ = +0.20 ‰ (median = +0.22 ‰) with low dispersion (2σ = 1.79 ‰). Archean samples are particularly depleted with respect to $\delta^{18}O_{carb}$, with a remarkably low mean of −12.3 ‰ (median = −11.8 ‰) and 2σ of ±9.34 ‰, compared to Holocene samples that are close to the PDB reference material (mean = −1.18 ‰, median = −0.12 ‰, 2σ of ±8.71 ‰). Holocene samples again have the widest isotopic variability (spanning a range of 26.1 ‰ in total), due in part to some exceptional present-day microenvironments that do not appear to be well-represented in the ancient rock record (see section 3.3.3 below).

The microbialite stable isotope results from this study are compared to a larger literature dataset comprised of isotopic data from 24,467 carbonates as compiled by Havig et al. (2017); data largely from Schopf, 1983; Hayes et al., 1983; Shields and Veizer, 2002; and Prokoph et al., 2008). This compilation reveals that carbonates on a global scale exhibit a wide range of signatures, spanning −24.7 to +18.0 ‰ in $\delta^{13}C_{carb}$ (median = +0.54 ‰) and from −30.4 to +4.23 ‰ in $\delta^{18}O_{carb}$ (median = −7.30 ‰). Comparison of our microbialite data with this larger body of data available in the literature permits an evaluation of whether the carbonate microbialites from the MNHN Microbialite Collection record previously recognized trends in carbonate isotopic compositions worldwide. In other words, whether microbialites may serve as reliable records of the isotopic evolution of Earth's surface reservoirs.

3.3.1. The stable carbon isotope record of carbonate microbialites

The $\delta^{13}C_{carb}$ values of the MNHN Microbialite Collection average around 0 ‰ across geological time (Fig. 5A). Carbonate data compiled from literature show the same average of around 0 ‰ as the microbialite data, with a similarly restricted $\delta^{13}C_{carb}$ range for Archean samples (i.e., 2σ = ± 4.47 ‰ for Archean carbonate data from literature vs. ± 1.79 ‰ for Archean microbialites). If globally representative, $\delta^{13}C_{carb}$ values around zero are conventionally attributed to “typical” Earth surface carbon cycling driven by biological CO_2 fixation and sedimentary carbon burial in a ratio of around 1:4, while extreme $\delta^{13}C_{carb}$ values are interpreted as periods of either elevated productivity and organic carbon burial (in the case of positive C isotope excursions), or enhanced organic matter remineralization (in the case of negative C isotope excursions). Importantly, the compiled carbonate data highlight some of Earth's most important carbon isotope excursions, notably the ca. 2.2 Ga Lomagundi-Jatuli Event (LJE; Schidlowski et al., 1976; Melezhik and Fallick, 1996) and the ca. 600 Ma Terminal Neoproterozoic Shuram-Wonoka Anomaly (SWA) (Fike et al., 2006; see Halverson et al., 2010, for review) (Fig. 5A). Samples in the MNHN Microbialite Collection also capture these excursions; notably the positive LJE excursion in microbialite samples from the Nash Fork Formation of the Wyoming Craton, as previously recognized by Bekker et al. (2003), and the negative SWA excursion in the Oued Djouf Formation of the Hank-Fersiga Area of the Taoudéni Basin, Algeria (Deynoux et al., 2006) where it had been previously recognized by Álvaro et al. (2007). While the causes of these major Earth surface carbon cycle perturbations remain highly debated (e.g., Prave et al., 2021), it can be concluded that whatever drove these major excursions clearly affected carbonate microbialites as well.

The microbialite $\delta^{13}C_{carb}$ record presented here also contains some notable deviations from known lacustrine and marine records that warrant special consideration. First, marine stromatolites from the Bonne River Formation of the Hoyoux Group of Warnantian age (ca. 326 Ma) (Belgium; Aretz and Chevaliers, 2007) show consistently low $\delta^{13}C_{carb}$ values, ranging from −8.95 ‰ to −10.3 ‰; such values are unprecedently low for the entire Mississippian (c.f. Bruckschen et al., 1999) and indeed highly atypical for most of the Phanerozoic. Such departures almost certainly relate to environments with highly local processes driving atypical carbon cycling (see also section 3.3.3), in this case likely by a shallow-water or porewater dissolve inorganic carbone (DIC) pool that was heavily influenced by organic matter remineralization and likely methanotrophy. Indeed, anaerobic oxidation of methane is implicated in the formation of similarly-light carbonates (spanning −8.31 ‰ to −11.0 ‰ in the MNHN samples analyzed) from the Upper Jurassic (ca. 146 Ma) Münder Formation (Germany) that formed in an evaporitic marine setting (Arp et al., 2008). These two examples of extreme light C isotope enrichment in Phanerozoic marine carbonate microbialites (the lowest marine (blue) data points, between 500 and 50 Ma, in Fig. 5A) highlight the propensity for microbialites in specific cases to record extreme values due to localized and exotic carbon cycling, even if for the most part microbialites provide a C isotope record that is comparable to sedimentary carbonates across geological time.

Intriguingly, the available dataset from the MNHN Microbialite Collection highlights the absence of significant differences between marine and lacustrine samples (Fig. 5A; mean and $2\sigma_x$ values of −0.47 ± 0.43 ‰ vs. +0.77 ‰ ± 0.41 ‰, respectively). This indicates that, other than specific cases (such as those discussed immediately above as well as below in section 3.3.3) where intense local productivity or methane escape locally drives the DIC pool to extreme values, the overarching control for setting $\delta^{13}C_{carb}$ in microbialites deposited throughout Earth's history is the rapid equilibrium between ambient DIC and atmospheric CO_2. Thus, excepting certain specific cases of intense and localized carbon cycling, carbonate microbialites in both marine

and lacustrine settings appear to be reliable recorders of global carbon cycling.

3.3.2. The stable oxygen isotope record of carbonate microbialites

The trend to heavier $\delta^{18}O_{carb}$ compositions over geological time is clearly visible in the literature compilation dataset (Fig. 5B). Archean carbonate data from literature show a mean $\delta^{18}O_{carb}$ value of −12.3 ‰ (median = −11.8 ‰, 2σ = 9.34 ‰), while Proterozoic carbonates display a mean of −6.57 ‰ (median = −5.67 ‰, 2σ = 7.12 ‰), and Phanerozoic carbonates average around −3.02 ‰ (median = −2.69 ‰, 2σ = 8.58 ‰). Even if the mean and median $\delta^{18}O_{carb}$ values overlap within error for sedimentary carbonates across these different eons due significant dispersion in the data, and the same is true for data from MNHN Microbialite Collection, both effectively record the same macroevolutionary trend through time towards higher $\delta^{18}O_{carb}$ values (Fig. 5B).

The MNHN Microbialite Collection includes Archean lacustrine microbialite samples from the 2.7 Ga old Tumbiana Fm. and our new analyses confirm previous reports of lacustrine carbonate $\delta^{18}O$ values in the Archean that are as light as their marine counterparts (Thomazo et al., 2009 and references therein; Fig. 5B). We suggest that this is best explained as reflecting a global hydrological cycle anchored at $\delta^{18}O$ values lighter than those set by oceanic hydrothermal circulation, as it occurs today. This inference is consistent with recent studies highlighted in the introduction indicating marine $\delta^{18}O$ values near −8 ‰ ca. 2.4 to 2.0 Ga, whether via the temperature-insensitive iron oxide $\delta^{18}O_{ox}$ record (Galili et al., 2019) or the occurrence of marine barium sulfates in the Turee Creek Group with abnormally light $\delta^{18}O_{carb}$ values (Killingsworth et al., 2019). While the possibility that both marine and lacustrine samples of Archean age were both altered to lower $\delta^{18}O_{carb}$ values by metamorphic fluids cannot be entirely excluded, the similarity in $\delta^{18}O_{carb}$ between lacustrine and marine microbialite samples collection is entirely consistent with the "evolving hydrological cycle" interpretation and underlines the potential for resolving the issue of highly depleted $\delta^{18}O$ values in Precambrian sediments through the careful comparison of marine and lacustrine deposits, and possibly new analytical approaches (e.g., triple O isotopes of oxyanions in marine vs. lacustrine microbialites).

For both the $\delta^{18}O$ and $\delta^{13}C$ datasets (Fig. 5), it is clear that the MNHN Microbialite Collection favors different environments at different times in Earth's history: Precambrian samples tend to be marine, whereas Phanerozoic microbialites often occur in freshwater. Considering that there exists significantly less data for Precambrian stromatolites relative to their Phanerozoic counterparts or sedimentary carbonates in general, whether this feature is a true reflection of the evolution of microbialite-forming niches, or stems from biases related to recognition or preservation of lacustrine environments in deep time, warrants future consideration. Regardless, as seen in Fig. 5 and explored further below, it is thus expected that modern microbialites may show greater deviations from the near-zero $\delta^{18}O$ values proscribed by marine carbonate deposition, for example towards lighter values driven by the influence of meteoric or hot spring waters.

3.3.3. Local effects on carbonate microbialite C and O isotope compositions: insights from quaternary examples

At the broadest scales, carbonate microbialites worldwide record a history of evolving C and O isotope compositions that is similar to their non-microbialite carbonate counterparts (see sections 3.3.1 and 3.3.2). At the same time, they may be more prone to local effects due to their shallow-water photic zone habitat and the fact that they often occur under extreme hydrological conditions (e.g., highly evaporitic settings, hydrothermal springs) and/or in association with high productivity and exotic carbon cycling. Even more so today, widespread predation limits modern microbialite occurrence, whereas in the past, more extreme oceanic and climatic conditions, as well as a lack of predation, favored microbialite formation in the semi-restricted and open-marine realm. Recognizing extreme depositional settings such as highly evaporitic lagoons or hydrothermally influenced fresh waters is not always straightforward from outcrop observation, stratigraphic records, or elemental composition; for this reason, paleoenvironmental classification beyond "marine" vs. "non-marine" is imprudent for many ancient microbialites in the MHNH collection. However, modern microbialite occurrences are much better constrained by simple observation of the environments in which they are found. In this section we examine Quaternary carbonate microbialites in the MNHN collection for which their precise depositional context is well constrained (Supplementary Table 2) and for which specific processes affecting local carbon and oxygen cycling may be resolved.

Indeed, Quaternary carbonate microbialites may show a wide range of $\delta^{13}C_{carb}$ and $\delta^{18}O_{carb}$ in a single deposit, and also show some remarkable grouping patterns in $\delta^{13}C_{carb}$ vs. $\delta^{18}O_{carb}$ space that may testify to the unique climatic, chemical, or biological conditions intrinsic to their depositional environments (Fig. 6). With respect to carbon, the modern open marine microbialites analyzed are centered around 0 ‰ in $\delta^{13}C_{carb}$, but span a surprisingly large range, from −5.19 ‰ to +5.02 ‰. However, most of the Quaternary carbonate microbialites analyzed are isotopically heavier than 0 ‰; this includes samples from semi-restricted marine settings and coastal lagoons as well as saline and (saline-) volcanic crater lakes. These may all be explained to first order by biological removal of carbon by biomass and removal of isotopically light carbon from the local DIC pool. Indeed, in restricted and hypersaline settings and especially at warmer temperatures, the solubility of CO_2 is depressed such that the DIC pool may become small relative to biological demand, leading to an isotopically heavy DIC pool that may also be expressed in isotopically heavy $\delta^{13}C_{org}$ signatures of co-eval biomass (Schidlowski et al., 1984). In the alkaline volcanic crater lakes Atexcac Lagoon (Mexico; Pleistocene age) and Dziani Dzaha (Mayotte, Holocene

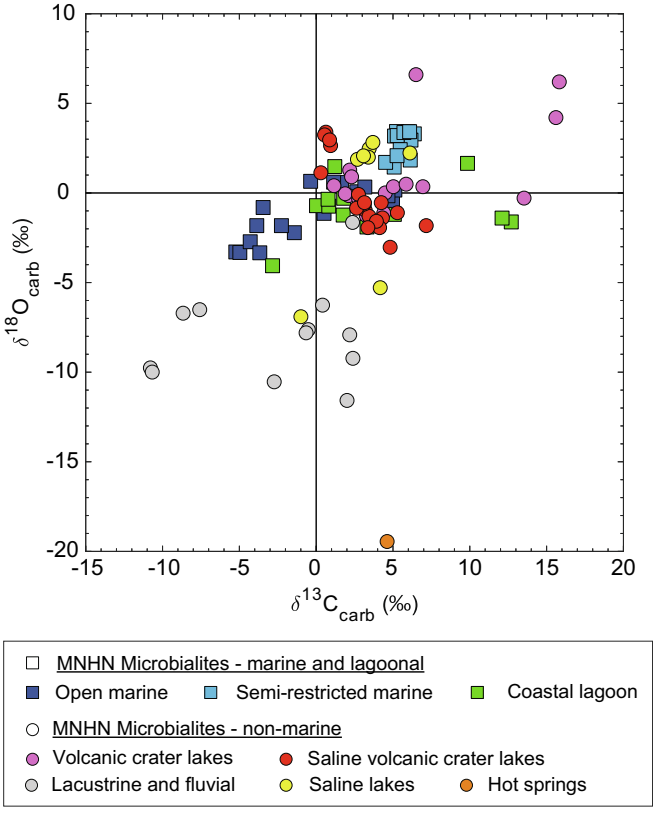

Fig. 6. Cross plot of $\delta^{13}C_{carb}$ (VPDB) vs. $\delta^{18}O_{carb}$ (VPDB) of Quaternary carbonate microbialite samples analyzed from the MNHN Microbialite Collection classified by their depositional environment. A complete list of the 99 samples plotted is provided in Supplementary Table 2.

age), carbonates are enriched in $\delta^{13}C_{carb}$ by over +13 ‰ (purple points at right in Fig. 6) relative to modern marine carbonates. Similarly, carbonate microbialites analyzed from the coastal lagoon Lagoa Salgada (Brazil, Holocene age; green points at right in Fig. 6) show $\delta^{13}C_{carb}$ values up to +12.5 ‰, consistent with values of greater than +16 ‰ reported in literature from this site (Birgel et al., 2015; Hu et al., 2023). At the two latter localities, the extreme positive $\delta^{13}C_{carb}$ values have been interpreted to represent high primary productivity coupled with efficient methanogenesis and the escape of isotopically light carbon to the atmosphere via methane emission (Birgel et al., 2015; Cadeau et al., 2020). Surprisingly, at Atexcac Lagoon, where dissolved organic carbon constitutes an important fraction of the total dissolved carbon pool, no evidence for important methanogenesis is reported, and the aqueous DIC pool is near 0 ‰ (Havas et al., 2023); the mechanism responsible for the elevated $\delta^{13}C_{carb}$ values measured at this site remains unknown.

Lacustrine and fluvial carbonate microbialites (grey points in Fig. 6) present $\delta^{13}C_{carb}$ values that tend to be isotopically lighter than marine carbonate due to the mixed nature of their carbon sources; for rivers and lakes fed by catchments draining predominantly carbonate bedrock, their carbonates tend to be isotopically heavier, while catchments with organic matter as an important source of alkalinity tend to show isotopically lighter $\delta^{13}C_{carb}$ values. The modern carbonate microbialites showing the lowest $\delta^{13}C_{carb}$ values (down to −10.7 ‰) are from Lake Lunz (Austria, Holocene age), an oligotrophic mountain lake where internal cycling of carbon between the organic and DIC pools represent only a minor component (ca. 0.5%) of the annual carbon flux in and out of the lake, both of which are strongly dominated by riverine DIC inflow and outflow (Ejarque et al., 2021). While $\delta^{13}C_{DIC}$ data is not available for neither the lake nor its main inlet (the Oberer Seebach stream), the catchment drains a forested setting with humic-rich soils, and contributions from organic carbon to the lake DIC pool are likely responsible for the light isotopic compositions measured here.

Lacustrine and fluvial microbialites also present among the lowest and most variable $\delta^{18}O_{carb}$ values, which are in these cases controlled by the local hydrological context (latitude, and to a lesser extent, altitude). Modern carbonate microbialite from Mammoth Hot Springs, Yellowstone National Park (orange point in Fig. 6), represents an extreme case (−19.4 ‰) of local hydrological control (the presence of hot spring waters). Microbialites in isolated water bodies stand in contrast with carbonate microbialites from modern marine and lagoonal settings, which range from −4.04 to +3.46 in $\delta^{18}O_{carb}$, buffered close to seawater values and with a tendance towards higher values in cases where isotopic distillation during evaporation drove the entire water body to isotopically heavy $\delta^{18}O$ compositions. For example, in the MNHN Microbialite Collection, Quaternary stromatolites from Mexican lakes such as Atexcac and Alchichica have high $\delta^{18}O$ values (+6.23 and + 6.63 ‰, respectively) that they go beyond those reported in the carbonate literature data compilation employed herein that contains over 24,000 analyses (maximum value of +4.23 ‰); this is a clear reflection of their extreme depositional environment. Interestingly, while carbonates can be deposited at a variety of water depths, microbialites are generally restricted to the shallow waters in the photic zone, such that they may be exposed to greater variability in water sources and surface water temperatures, as illustrated by the above cases.

3.4. Rare Earth Element records of evolving microbialite depositional environments

In the following section, data obtained by REE analyses of the MNHN Microbialite Collection are compared against a compilation of 5131 carbonates from two major data sources that have been recently published as open datasets in coordination with this work. The first is comprised of sedimentary carbonate major and trace element data compiled from literature, totaling 4476 samples and including over 60 literature sources, supplemented with additional data from diverse microbialites the authors have amassed over the years analyzed using the same weak-leach technique employed herein (Lalonde et al., 2024). The second is a large compilation ($n = 655$) of new weak-leach REE data that was recently made available as an open dataset in the context of an independent study (Patry et al., 2024) on Mesoarchean stromatolitic carbonates at three sites of the Superior Province (Canada): Red Lake (2.87 Ga), Woman Lake (2.86 Ga) and Steep Rock Lake (2.80 Ga). These large datasets permit us to evaluate the representativity of the REE systematics observed in the MNHN Microbialite Collection with respect to global sedimentary carbonates and, in turn, the utility of REE tracers in microbial carbonates more generally for paleoenvironmental reconstruction. All REE spectra and most REE anomaly indicators (unless otherwise indicated) are reported as shale-normalized to PAAS, as described in section 2.

3.4.1. REE spectral features in carbonate microbialites

In Fig. 7, PAAS-normalized spectra are presented for samples that were selected for the particularly clear REE characteristics that they show in relation to diverse depositional paleoenvironments represented by the carbonate microbialites of the MNHN Microbialite Collection (see Supplementary Table 3). Many of the characteristic REE spectral features of modern seawater, namely LREE/HREE enrichment, positive La/La* and Gd/Gd* anomalies, and suprachrondritic Y/Ho ratios, are visible in Archean microbialites deposited under open ocean marine conditions (light blue spectra, Fig. 7), such as from the Campbellrand-Malmani carbonate platform (South Africa) and Woman Lake Assemblage (Canada). The importance of local hydrothermal inputs to microbialite-forming environments is exemplified by the presence of strong positive Eu/Eu* anomalies in carbonate microbialites from the Red Lake Greenstone Belt and Nash Fork Formation (navy blue spectra, Fig. 7). Carbonates from the 3.75 Ga Isua Greenstone Belt, for which claims of microbial influence are currently controversial (e.g., Nutman et al., 2016; Allwood et al., 2018), are also characterized by important positive Eu/Eu* anomalies that testify to deposition from hydrothermally influenced seawater (the top spectrum among the 3 navy blue ones in Fig. 7). By contrast, lagoonal and shallow marine environments may not express typical seawater signatures but instead often present flat REE patterns with slight MREE enrichment and muted to absent La and Y anomalies. These include carbonate microbialites from Mari Ermi (Sardinia), North Caicos (the Caribbean), and Shark Bay (Australia), which are presented as the uppermost green spectra in Fig. 7. In these environments, REE are dominated by the riverine flux that generally (but not always; Merschel et al., 2017) bears a flat continental-type REE pattern when normalized to PAAS.

In the lacustrine samples of the collection, a large proportion of microbialites come from saline-alkaline lakes and tend to present a flat pattern with elevated REE concentrations (yellow spectra, Fig. 7). The yellow spectra plotted in Fig. 7 are examples of microbialites from Lake Logipi (Kenya, Holocene), El Molino at Agua Clara (Bolivia, 70 Ma), Cedar Mountain (USA, 125 Ma), and Green River (USA, 40 Ma). Remarkably, stromatolites from the intracontinental lake in the Richat Structure (Mauritania) show exceptionally high REE concentrations and a pattern clearly enriched in MREE (grey spectrum, Fig. 7). Volcanic crater lake samples represented by Rincón de Parangueo, Atexcaca, Alberca de Los Espinos (Mexico) and Lake Tauca (Altiplano of Bolivia) show large positive Eu anomalies, significant high HREE enrichment, a small positive Y anomaly, and negative Ce anomalies (purple spectra, Fig. 7). These characteristics are remarkably seawater-like and are also observed in stromatolite samples from Lamalou-les-Bains (France) that were deposited in a continental setting influenced by modern hydrothermal fluids (red spectrum, Fig. 7). Alkaline lake waters are also known to present seawater-like patterns (Kreitsmann and Bau, 2023), although this was not observed in the MNHN carbonate microbialite samples from saline-alkaline lakes. Interestingly, a distinct pattern is observed in Mammoth Hot Springs stromatolites from Yellowstone National Park (USA) that precipitated in a geothermal environment, with a clear positive anomaly in both Eu and Gd, accompanied by a slight

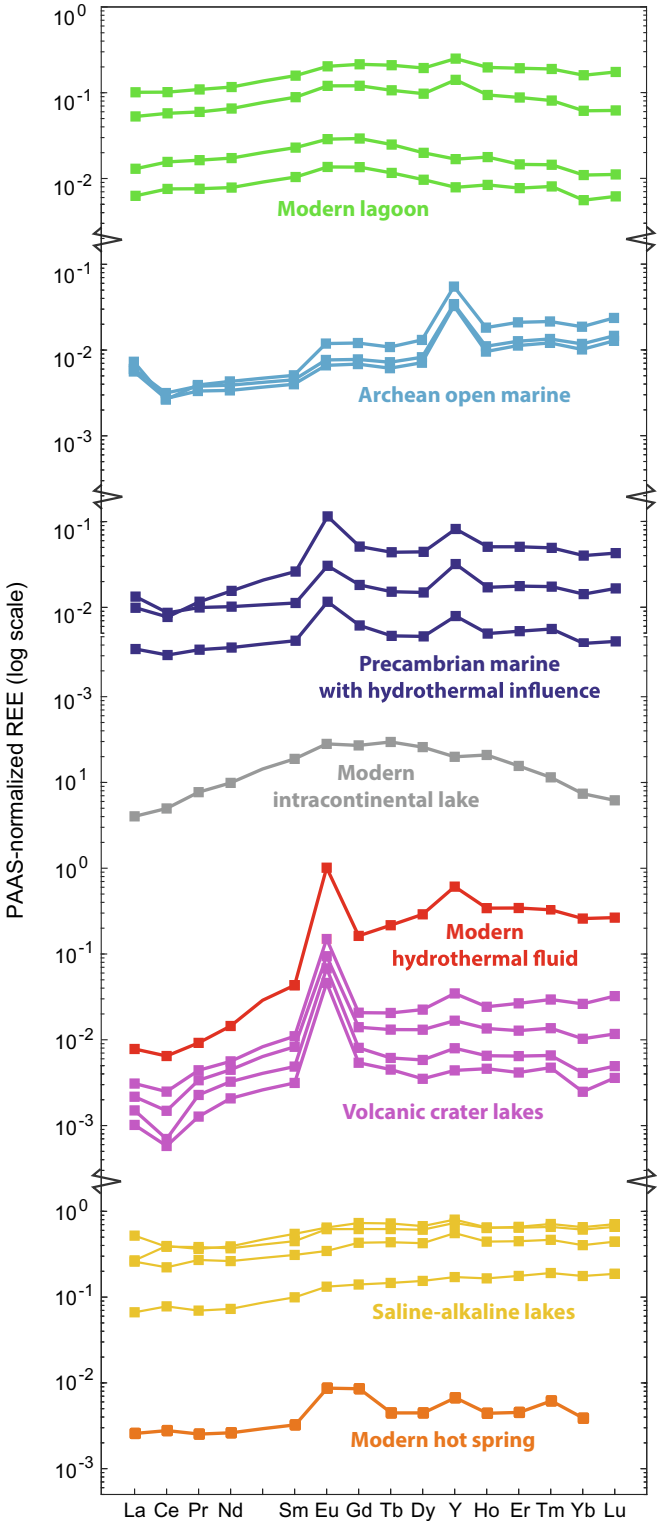

Fig. 7. PAAS-normalized REE spectra from the MNHN carbonate microbialite dataset of samples selected for their high degree of representativity (with clear, environment-specific features) of different end-member depositional environments. The 21 selected samples are specified in Supplementary Table 3; we emphasize that most samples in the dataset do not show features as clear as these selected examples. Some REE anomalies of interest, specifically those affecting cerium (Ce), europium (Eu), and yttrium (Y), are noted with vertical dashed lines.

positive anomaly in Y (orange spectrum, Fig. 7).

As seen above, REE in stromatolitic carbonates are powerful paleoenvironment tracers that may reveal a variety of specific processes operating in different aqueous environments once other confounding factors (e.g., detrital contamination, phosphate mineralization) can be eliminated. Some overlap in features clearly occurs, and sometimes similar settings may provide contrasting signals. Indeed, the spectra presented in Fig. 7 were selected as representing some of the most clear-cut examples; we highlight to the reader that the greater REE dataset associated with this article is somewhat noisy based on visual inspection of the hundreds of spectra generated. Nonetheless, the above examples effectively illustrate how microbialites may indeed record REE spectral features that are informative with regards to their paleodepositional settings.

3.4.2. REE anomalies in carbonate microbialites: perspectives from the MNHN microbialite collection

An overview of total REE abundances and REE anomaly indicators determined for the MNHN Microbialite Collection are presented as a function of age in Fig. 8. Total REE concentrations using the weak acetic acid leach technique show a median value of 20.8 ppm, but due to some extreme values (e.g., up to 2000 ppm of REE for the Holocene stromatolites from the hydrothermally influenced Richat Structure in Mauritania), the mean value is significantly higher at 50.1 ppm. Total REE concentrations in the MNHN collection are variable as a function of age, with generally low concentrations in Paleoarchean stromatolites, elevated but secularly decreasing values from the Mesoarchean to the Paleoproterozoic, and a greater range in values from the Neoproterozoic through the Cambrian (Fig. 8A). The dichotomy between the Archean and post-Archean samples may be related to a preponderance of highly pure chemical sediments composing Archean stromatolites deposited under more sediment-starved or open-ocean conditions, vs. their younger equivalents which tend to include more evidence of sediment re-working and grain binding/trapping. Yet higher total REE in the Cambrian could similarly be a consequence of the restriction of stromatolites to shallow-water or highly evaporitic systems subject to even greater detrital sourcing. That said, it is important to note that carbonate mineralogy (e.g., aragonite vs. calcite vs. dolomite) as well as fluid composition (pH, carbonate content, environmental-specific REE load) may have equally contributed or even controlled the evolving REE contents of microbialites through time.

PAAS-normalized europium anomalies in the MNHN Microbialite Collection average Eu/Eu* = 1.50 and show important secular variation with time (Fig. 8B). Strong positive Eu anomalies are clearly expressed in Archean to Paleoproterozoic microbialites, regardless of normalization (here normalized to PAAS; note that chondrite-normalized values would be lower by a factor of 0.61). These important Eu anomalies almost certainly reflect local sources of high-temperature hydrothermal fluids in most marine depositional environments at the time (e.g., Bau and Dulski, 1996a, 1996b; Bolhar et al., 2004; Allwood et al., 2010; Kamber et al., 2014). Archean samples show significantly higher anomalies, around 2.80 for the Eo- to Paleo-archean, with values up to 3.38; values then generally decrease until the Mesoproterozoic after which they remain generally low. This record is remarkably consistent with the evolution of Eu/Eu* in Precambrian iron formations, which, with the exception of a notable peak in Eu/Eu* values ca. 2.7 Ga, similarly show waning Eu/Eu* throughout the Archean and earliest Paleoproterozoic (Viehmann et al., 2015).

In general, the oldest microbialites in the MNHN collection of Paleo- to Meso-archean age show a restricted range in Ce/Ce* values, rarely lower than 0.95 nor higher than 1.05, and a median close to 1 (Fig. 8C), consistent with the general absence of oxidative Ce processing at that time. That said, the most extreme Ce/Ce* values are remarkably variable in MNHN collection carbonate microbialites deposited prior to the GOE. While some carbonate microbialites in the collection come from previously-proposed oxygen oases for which the REE spectra appear

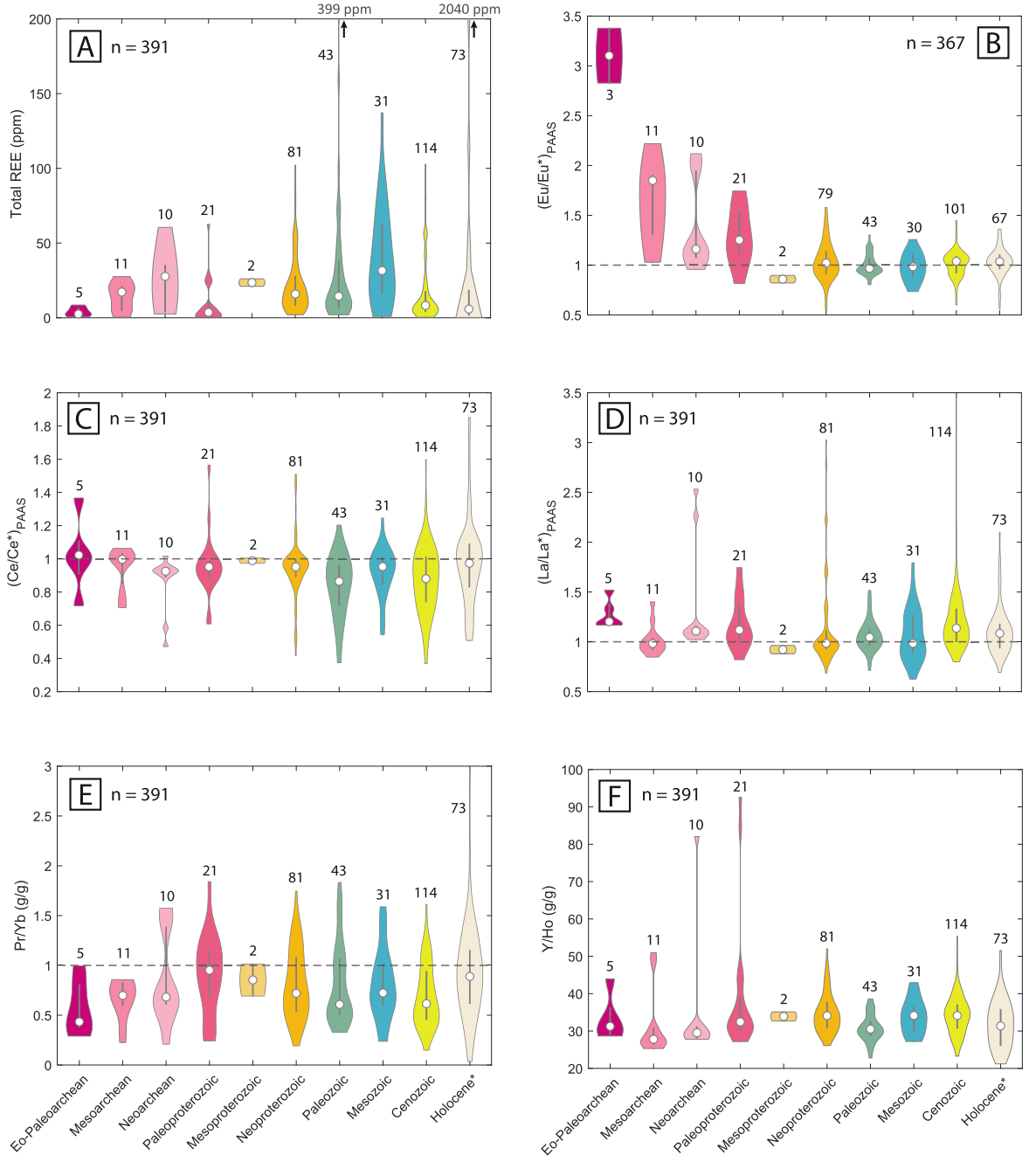

Fig. 8. Violin plots summarizing multiple features of the REE data from the MNHN Microbialite Collection: total REE concentrations (A), PAAS-normalized europium anomalies (B), PAAS-normalized cerium anomalies (C), PAAS-normalized lanthanum anomalies (D), praseodymium to ytterbium ratios (E), and yttrium to holmium ratios (F). Samples are classified according to age, with Holocene samples explicitly separated from the rest of the Cenozoic samples.

undisturbed (e.g., 2.80 Ga Steep Rock Lake; Riding et al., 2014), post-depositional Ce/Ce* fractionation as the result of surface weathering appears to have affected some ancient chemical sediments examined in other studies (Planavsky et al., 2020) and, thus, caution is warranted in interpreting these data as redox signatures without geochronological constraints on Ce oxidation (Bonnand et al., 2020). Median Ce/Ce* anomalies in the MNHN collection samples are below one in the Neoarchean and Paleoproterozoic, rise slightly in the Meso- and Neoproterozoic, and become more variable afterwards, with a significantly expanded spread in Ce/Ce* values beginning in the Neoproterozoic. This increasing range in Ce/Ce* values (both positive and negative) indicates that microbialite depositional environments were generally more oxidizing with respect to Ce; part of this trend may have been driven by the increasing importance of Mn-oxide minerals in Earth surface environments (Maynard, 2010; Robbins et al., 2023) and their role as catalyzers for Ce oxidation.

As introduced in section 1.3.2, the presence of La/La* anomalies, Gd/Gd* anomalies, suprachrondritic Y/Ho ratios, and the relative enrichment of HREE over LREE (evaluated here using the Pr/Yb ratio) are all considered seawater REE signatures that are recognizable in chemical sediments as far back as Earth's oldest sediments deposited ca. 3.7 Ga ago (Bolhar et al., 2004). The MNHN collection REE dataset permits us to evaluate in a broad fashion how these signatures in ancient carbonate microbialites have evolved over geological time. Box plots of

La/La* anomalies, Pr/Yb ratios, and Y/Ho ratios in the MNHN collection samples are presented over geological time in Fig. 8D, E, and F, and show remarkable variation. Both La/La* and Y/Ho ratios are elevated in Eo- to Paleo-archean samples, drop significantly in the Mesoarchean, and then rise until the Paleoproterozoic, after which La/La* ratios remain relative static around 1 until the Cenozoic, while Y/Ho ratios show more variability from the Neoproterozoic onwards. For all periods in the MNHN dataset, median La/La* values are below 1.20, and median Y/Ho ratios remain close to continental crust value of 26 (Kamber et al., 2005), not depassing 35. Intriguingly, the carbonate microbialite Y/Ho record is somewhat different than that for banded iron formations, which show generally higher and less variable Y/Ho throughout Earth history (Ernst and Bau, 2021), which may be a reflection of the variety of microbialite-forming niches in deep time vs. the generally deep-water locus of precipitation of the latter.

Finally, there appears to be significant evolution in the Pr/Yb ratio of carbonate microbialites across the Archean that generally stabilizes in the Proterozoic onwards (Fig. 8E). The HREE enrichment of seawater is driven by pH-dependent aqueous carbonate complexation of lanthanides (Byrne and Kim, 1990), and this early secular evolution in carbonate microbialites may reflect changes in ocean alkalinity and pH in responses to evolving atmospheric CO_2. That said, the evolution in the composition of rocks available at Earth's surface from mafic to felsic over this time window may have also played a role in the apparently higher degree of HREE enrichment in deep geological time previously observed in Archean chemical sediments (Kamber, 2010) and reaffirmed here through the MNHN collection carbonate microbialite data.

The preponderance of important positive Eu anomalies in the ancient sedimentary carbonate record in general is also evident in Fig. 9A, where the MNHN collection data (circles) are plotted against compiled literature data for sedimentary carbonates worldwide. Here, Eu/Eu* is plotted against Pr/Yb as an indicator of LREE vs. HREE enrichment; HREE enrichment being a classic seawater REE signature (see above and below). It can be seen that Paleo- and Meso-archean carbonates generally dominate the high Eu/Eu*, low Pr/Yb (seawater) pole. Looking at the data plotted as a function of marine vs. lacustrine depositional settings (Fig. 9B), one important exception is immediately apparent in the form of a cluster of Cenozoic microbialites with high Eu/Eu* values and low Pr/Yb despite their lacustrine origin. This underlines that while global Eu/Eu* in both the literature carbonate REE data as well as the MNHN collection carbonate microbialite data indicate a waning importance of high-temperature hydrothermal fluids in carbonate sedimentary environments over geological time, high Eu/Eu* values combined with other seawater signatures may not necessarily be diagnostic of hydrothermally influenced marine deposition, but rather are simply consistent with it.

When plotted against Y/Ho ratios in (g/g) as an indicator of open marine vs. freshwater or closed-basin conditions (Fig. 9C), it can be seen that Archean to Paleoproterozoic carbonate microbialites dominate at Y/Ho values above 50.0 while showing generally near-zero to slightly negative Ce/Ce* values, while younger carbonate microbialites generally show Y/Ho values below 50.0 (Fig. 9C) and are characterized by highly variable Ce/Ce* values. Recast in the context of known depositional environments (lacustrine vs. marine; Fig. 9D), the MNHN collection data reveal that marine and lacustrine microbialites deposited since the Paleoproterozoic show comparable ranges in both Ce/Ce* and Y/Ho ratios. This is significant for two reasons. First, it demonstrates the applicability of Ce/Ce* as a redox tracer in both lacustrine and marine microbialites (e.g., Wilmeth et al., 2022). Second, it indicates that some REE proxy indicators thought to represent deposition under marine conditions, such the Y/Ho ratio, may be less diagnostic than previously assumed for the freshwater vs. marine origin of carbonate microbialites, as we explore further below.

Importantly, plots of La/La* vs. Y/Ho for the dataset, combined with carbonate data from literature (Fig. 9E), reveal that carbonates deposited in the Archean, including microbial carbonates (the majority of compiled data for Archean carbonates are from microbialites; Patry et al., 2024), tend to show scaling in both La/La* and Y/Ho with increasing open seawater influence, likely reflecting their growth under more open-ocean conditions. Younger carbonate microbialites are predominately lacustrine or hypersaline/lagoonal, and are rarely represented in the "open-ocean" space in Fig. 9E and F, projecting instead more vertical arrays with a tendency for greater variation in La/La* than Y/Ho. While Phanerozoic carbonate microbialites rarely show the high La/La*, high Y/Ho open-ocean seawater signature of Archean carbonates, they none the less show more crustal-like signatures in lacustrine settings and more extreme La/La* (and to a lesser extent, Y/Ho) values in marine settings that tend to be predominantly lagoonal or hypersaline, which may explain their muted values compared to the expanded Archean range.

3.5. *Earth surface oxygenation recorded by redox-sensitive elements in ancient microbialites*

As developed in section 1.3.3, the enrichment of redox-sensitive elements such as Fe, Mn, U, Mo, and V in chemical and fine-grained clastic sedimentary rocks have proven potential for reconstructing the evolution of Earth's surface and marine redox conditions (Calvert and Pedersen, 1993; Russell and Morford, 2001; Wille et al., 2013; Robbins et al., 2016). In this section we examine the concentrations of these five elements in the carbonate microbialites of the MNHN Microbialite Collection with the specific goals of (1) revealing secular trends in their evolution and (2) comparing them to previously published records from other sedimentary lithologies to evaluate to what degree carbonate microbialites mirror other sedimentary records of Earth system change.

Carbonate microbialites from the MNHN Microbialite Collection present very high iron concentrations (Fe) in the Archean (mean = 5640 ppm, median = 3610 ppm), which decrease remarkably through the Proterozoic (mean = 3260 ppm, median = 2320 ppm), and finally reach lowest concentrations in the Phanerozoic (mean = 908 ppm, median = 209 ppm; Fig. 10A). Likewise, manganese concentrations (Mn) in collection samples are high during the Archean (mean = 2130 ppm, median = 2340 ppm), appear to increase across the Meso-to Neoarchean, and drop precipitously in the Paleoproterozoic (Fig. 10B). Mn concentrations remain elevated throughout the Proterozoic (mean = 1920 ppm, median = 529 ppm) relative to the Phanerozoic, which generally shows lower mean Mn concentrations with the exception of a notable peak in the Mesozoic (overall Phanerozoic mean = 901 ppm, median = 314 ppm). For both Fe and Mn, long tails representing rare Fe- and Mn-rich samples persist from the Neoproterozoic through to the Holocene, with maximal values tending to decrease over this period. The redox-sensitive trace elements U and Mo show the opposite trend, with increasing concentrations in carbonate microbialites over time (Fig. 10C and D). Their concentrations are depressed in the Precambrian (means = 0.32 ppm and 0.45 ppm, medians = 0.16 ppm and 0.12 ppm, for U and Mo, respectively), and show important but rare enrichments (long positive tails in Fig. 10C and D) associated with the Paleoproterozoic GOE, but otherwise remain relatively low until the Neoproterozoic, after which they show significantly and permanently increased mean and median concentrations (Phanerozoic means = 2.18 ppm and 0.45 ppm, medians = 1.08 ppm and 0.17 ppm, for U and Mo, respectively), with the most enriched samples reaching significantly higher values after the Paleozoic. Vanadium shows intermediate behavior between the two cases; like Fe and Mn, V concentrations show elevated median values during the Precambrian (1.71 ppm) relative to the Phanerozoic (1.35 ppm), but depressed means (2.84 ppm vs. 3.95 ppm for the Precambrian vs. Phanerozoic, respectively), as higher absolute concentrations in the most enriched microbialite samples are achieved during the Phanerozoic, a case similar to U and Mo.

A comparison of the carbonate microbialite data from the MNHN Microbialite Collection obtained for this study to literature data compiled from the analyses of ca. 4500 samples sedimentary carbonates

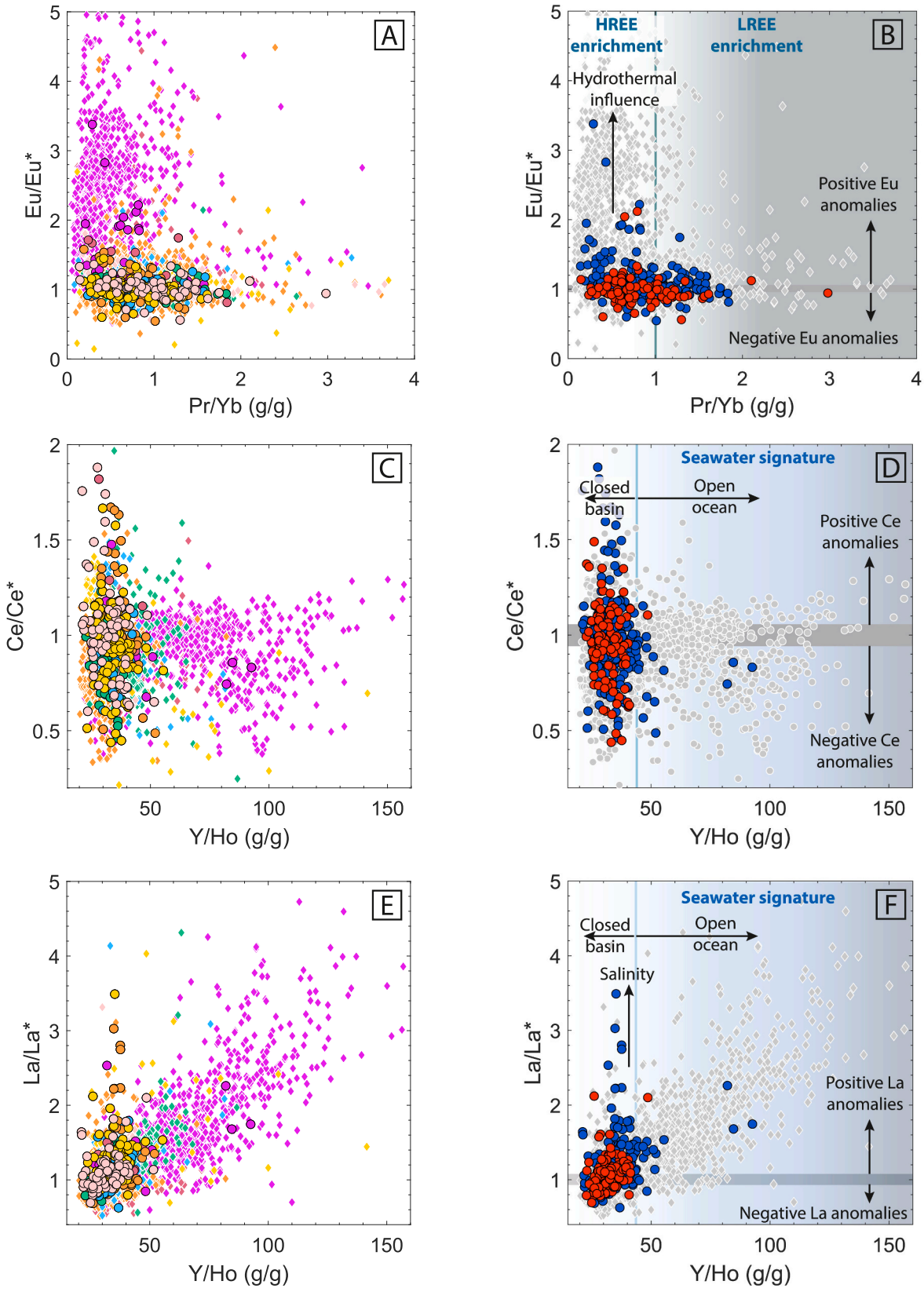

(caption on next page)

Fig. 9. PAAS-normalized europium anomalies plotted against praseodymium to ytterbium ratios (A and B as well as PAAS-normalized cerium anomalies (C and D) and lanthanum anomalies (E and F) plotted against yttrium to holmium. The plots in the first column (A, C and E) show data according to age, with Holocene samples plotted separately from Cenozoic samples. In the second column (B, D and F), the same data are plotted as a function of depositional environment (marine and non-marine) with additional annotations specific to each plot. The plots are composed of the same data from the MNHN Microbialite Collection presented in Fig. 8 (colored circles) and available REE data out of compiled literature data (from Lalonde et al., 2024 and Patry et al., 2024; colored and grey diamonds, 5131 samples compiled in total).

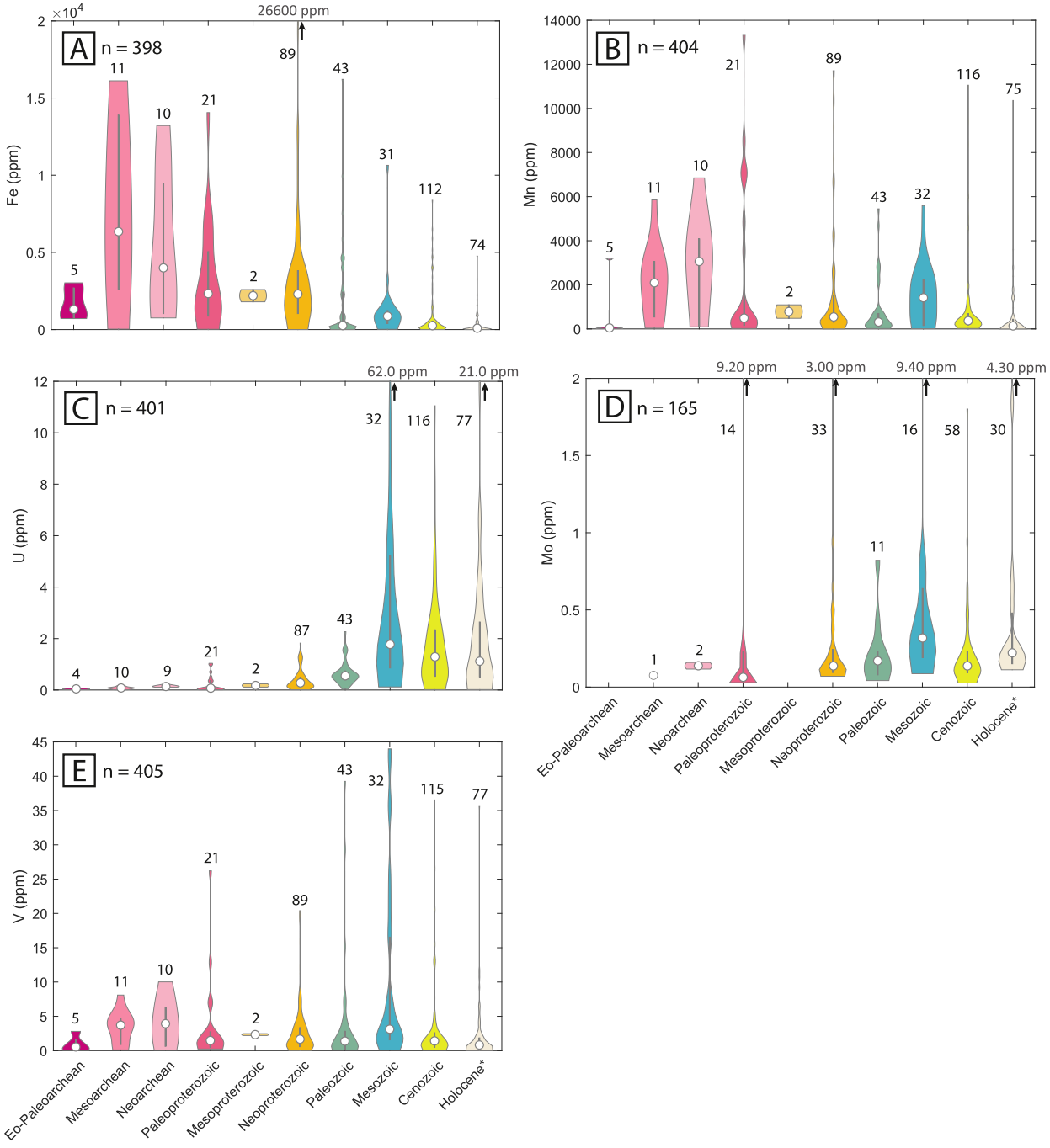

Fig. 10. Violin plots showing concentrations in the MNHN Microbialite Collection of selected redox-sensitive elements: iron (A), manganese (B), uranium (C), molybdenum (D), and vanadium (E). Samples are classified according to age, with Holocene samples explicitly separated from the rest of the Cenozoic samples.

worldwide (Lalonde et al., 2024) reveals some remarkable coherence between the two records (Fig. 11). While evolving carbonate mineralogy over geological time (e.g., from predominately dolomite to predominately calcite) may have played a role in these trends, Fig. 11A and B reveal that the overall trajectory of decreasing Fe and Mn in the MNHN microbialite data follow the well-recognized general paradigm of increasingly effective removal of these elements from aqueous environments over geological time (Maynard, 2010; Poulton and Canfield, 2011; Robbins et al., 2023). Both datasets are consistent with progressive Fe oxidation and Mn accumulation at Earth's surface leading up to

the GOE, during which iron oxidation was increasingly important but Mn oxidation was hindered due to a combination of insufficient oxidants and slow oxidation kinetics; after the GOE, both elements show important decreases as thresholds for efficient Mn oxidation were surpassed, giving rise to Earth's major Mn deposits in the Paleoproterozoic (Maynard, 2010; Robbins et al., 2023). In the specific case of Mn, the carbonate microbialite data inversely mirrors previously recognized trends in Mn mineral abundance (increasing with time) and their average oxidation state (increasing with time) in global crustal records (Hummer et al., 2022); it would thus appear that for the most part, Mn concentrations in carbonate microbialites are more of a reflection of the evolving seawater Mn reservoir (decreasing with time) than a locus of Mn oxidation as reflected by Mn mineral abundance and redox state (although exceptions likely exist, e.g., microbialites where localized Mn oxidation concentrates Mn beyond values expected from simple divalent Mn partitioning in carbonates). The picture is largely the same when the data are normalized to Al to distinguish detrital Fe and Mn sources (that should draw the data towards crustal Fe/Al and Mn/Al values) from true authigenic enrichments that lead to higher Al-normalized values (Supplementary Figs. 10 and 11). The MNHN collection data generally suggests that the Fe and Mn systematics of ancient microbialites are useful tracers of Earth surface redox evolution by their propensity to reflect ambient seawater Fe and Mn concentrations at the time of deposition.

The carbonate microbialites of the MNHN collection show a notable secular trend to higher U concentrations through geological time. This trend is broadly mirrored in the available carbonate literature data (Fig. 11C) and is in remarkable accordance with the evolution of U concentrations in black shales (Partin et al., 2013a) as well as banded iron formations (Partin et al., 2013b) over geological time. While this trend paints a coherent picture of progressive enrichment in seawater U concentrations over geological time, it's important to note that progressive U enrichment in carbonate microbialites extends equally to non-marine samples. This example illustrates how microbialites, by the diversity of their depositional environments both on land and at sea, may provide additional insight into global biogeochemical cycling beyond the marine realm. Uranium is a special case where its internal oceanic sources are near-negligible; U concentrations are near-zero in marine hydrothermal fluids and the near-entirety of marine U is supplied by oxidative continental weathering and riverine supply of U to the oceans (Dunk et al., 2002). The strong accordance between the marine and non-marine carbonate microbialite U records thus ties the evolving marine U reservoir directly to the evolution of continental weathering, opening new avenues of inquiry for examining the coupling between atmospheric O_2 concentrations, oxidative processes on land, and the response of the marine reservoir that is less accessible via chemical sedimentary records uniquely restricted to the marine realm, such as Precambrian iron formations or black shales.

Like uranium, moldybenum is largely supplied by oxidative continental weathering and is also characterized by sedimentary sinks that are highly redox-dependent (see section 1.3.3). While there are less Mo concentration data available due to the low abundance of Mo in sedimentary carbonates, especially prior to the Neoproterozoic, previous work on black shales, banded iron formations, and sedimentary carbonates reveals that sedimentary Mo enrichment across all of these lithologies has similarly strong potential for paleoredox reconstruction (see review by Thoby et al., 2019, for secular trends in compiled literature carbonate, shale, and BIF Mo concentration data). The concentrations of Mo in carbonate microbialites of the MNHN Microbialite Collection do not show an increase that is as clear as that observed for U over geological time; rather, it appears to be the highest Mo concentrations achieved that vary over time (c.f. violin plots in Fig. 10D (Mo concentrations) and Supplementary Fig. 10D (Mo/Al ratios)). Fig. 11D reveals significantly more variation for compiled literature carbonate Mo concentration data compared to the microbialite record presented here. Mo concentrations determined for the most ancient carbonate microbialites in the collection were often below detection (below ca. 20 ppb), consistent with isotope dilution data for Archean microbialites (Thoby et al., 2019). In contrast, there exists significant literature data reporting ppm-level Mo concentrations for Archean carbonates (Fig. 11D). Considering the low Mo abundances determined here using clean-laboratory techniques and high-resolution ICP-MS, and elsewhere using isotope dilution (Thoby et al., 2019), there is a strong possibility that Mo concentrations are overestimated in much of the available literature data.

Additionally, considering strong Mo isotope evidence for an important evolution in marine Mo cycling through geological time, it is curious that baseline Mo concentrations in carbonates remain low while the presumed trajectory of progressive Earth surface oxidation appears best reflected in highest Mo concentrations attained (c.f. long tails in Fig. 10D). One possibility is that contrary to the case for U, but similar to Mo enrichment in reducing sediments (see section 1.3.3), the enrichment in Mo in sedimentary carbonates may be highly dependent on the presence of H_2S (Romaniello et al., 2016). This leads to the possibility that “nugget effects”, or localized sources of Mo enrichment (e.g., sulfide minerals) in otherwise Mo-poor carbonate, may dominate both the literature carbonate and carbonate microbialite records presented here. Furthermore, contrary to the case for U, an important part of the modern marine Mo input flux is supplied by hydrothermalism (McManus et al., 2002). In deep geological time, when riverine Mo supplied by oxidative weathering was minimal (Anbar et al., 2007), it is possible that, contrary to the case for U, hydrothermal Mo fluxes sustained a minimal Mo reservoir, leading to a dampened signal for the evolution of Mo concentrations in marine carbonates through geological time. In this light, one interpretation of the expanded tails in the MNHN carbonate microbialite data is that localized microenvironments favoring Mo enrichment (e.g., sulfide-rich porewaters and diagenetic sulfide minerals) became more commonplace from the Paleoproterozoic onwards.

Available V concentration data for the MNHN Microbialite Collection indicates a tampered response to progressive oxygenation at Earth's surface (Fig. 11E), similar to the case for Mo. While V has proven redox proxy potential in shale records (e.g., Tribovillard et al., 2006; Sahoo et al., 2012), it remains little explored to date in the ancient sedimentary carbonate record, and the data presented here indicates an enrichment history similar to that of Mo, although further work is clearly warranted. In any case, the carbonate microbialite concentration records presented here of redox-sensitive trace metals such as Fe, Mn, and U, and to a lesser extent Mo and V, paint a picture of increasingly important oxidative processing in both terrestrial and oceanic environments. The coherence in these records with carbonate data compiled from literature reinforces the growing appreciation of carbonate microbialites as potentially powerful tracers of Earth redox evolution.

4. Conclusion

We present here the MNHN Microbialite Collection, a large collection of microbialite samples that reflects the evolving morphological and compositional diversity of microbialites worldwide and provides a unique carbonate geochemical record to evaluate the evolving paleoenvironmental signatures that microbialites may have recorded at different periods in geological time. We also provide an associated dataset comprised of over 400 high quality carbonate stable isotope (C and O) and trace element (including REE) analyses that we explore broadly through comparison to large datasets compiled from literature for carbonates worldwide. A major aim of this study was to evaluate the suitability of carbonate microbialites as recorders of the long-term biological and geological evolution at the Earth surface. In this regard, we demonstrate through this review that carbonate microbialites show comparable patterns of secular evolution through time in carbonate C isotopes (including major positive and negative excursions), O isotopes (with progressively increasing $\delta^{18}O$ values through time), and redox-sensitive trace elements. We further examine their evolving REE systematics with respect to carbonate literature data and find that ancient

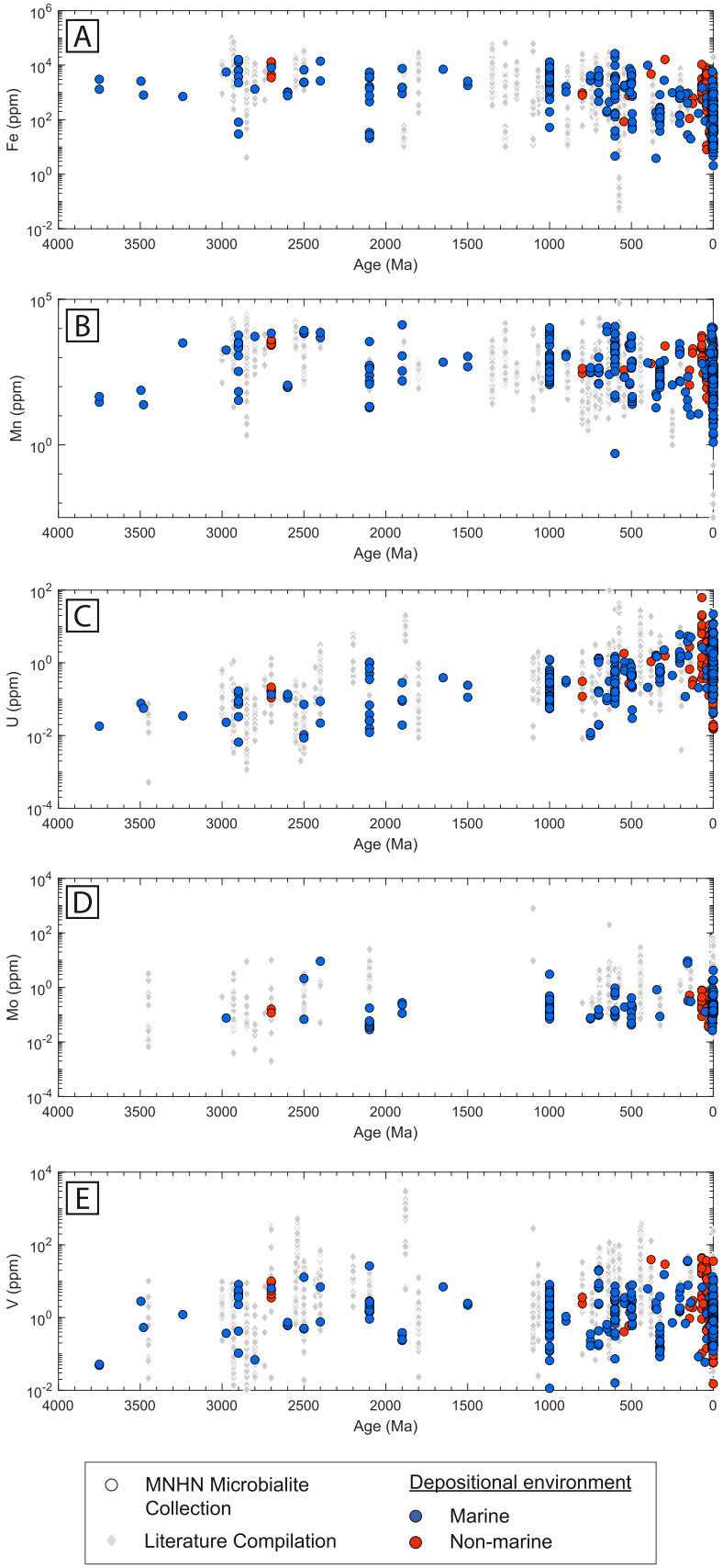

Fig. 11. Evolution of iron (A), manganese (B), uranium (C), molybdenum (D), and vanadium (E) concentrations in carbonate microbialites of the MNHN Microbialite Collection (colored circles, same data as presented in Fig. 10) compared to compiled literature data for carbonates through geological time (grey diamonds, available data for 5131 samples compiled).

carbonate microbialites, like sedimentary carbonates worldwide, record the REE systematics of their depositional environments, with respect to hydrothermal inputs, oxidative Ce processing, and the evolving importance of seawater-like fluids vs. more continentally sourced REE in hypersaline/lagoonal and lacustrine settings. Redox-sensitive trace element enrichments in carbonate microbialites are similarly consistent with literature carbonate data that testify to increasing oxygenation of Earth's atmosphere and oceans over geological time. Ultimately, the MNHN Microbialite Collection and associated datasets were established as a community sample and data resource at the service of microbialite researchers worldwide, and we hope that this review will stimulate further research and additional understanding of Earth's biological and geochemical evolution as preserved by microbial sediments worldwide.

Supplementary data to this article can be found online at https://doi.org/10.1016/j.chemgeo.2024.122239.

CRediT authorship contribution statement

Laurane Fogret: Writing – review & editing, Writing – original draft, Visualization, Software, Methodology, Investigation, Funding acquisition, Formal analysis, Data curation. **Pierre Sansjofre:** Writing – review & editing, Validation, Supervision, Resources, Project administration, Methodology, Investigation, Funding acquisition, Formal analysis, Conceptualization. **Stefan V. Lalonde:** Writing – review & editing, Validation, Supervision, Software, Resources, Project administration, Methodology, Investigation, Funding acquisition, Formal analysis, Conceptualization.

Declaration of competing interest

The authors declare that they have no known competing financial interests or personal relationships that could have appeared to influence the work reported in this paper.

Data availability

All data associated with this work are available from the EarthChem repository cited in the text (Fogret et al., 2024; Patry et al., 2024; Lalonde et al., 2024).

Acknowledgements

The authors would like to thank first and foremost all those who collected and provided samples to the MNHN Microbialite Collection (Supplementary Table 1) and especially Janine Sarfati, Karim Benzerara, and Russell Shapiro for their assistance and discussions regarding management of the collection. The authors thank the MNHN technical staff and specifically Caroline Noyes for her help with curation of the collection. The authors also thank Laureline Patry, Marie-Laure Rouget, and Yoan Germain for their assistance with HR-ICP-MS analyses, and Denis Fiorillo and Fabien Dewilde for their assistance with IRMS analyses. This work was supported by the European Research Council (ERC) under the European Union's Horizon 2020 research and innovation programme (grant agreement n° 716515 to S.V.L.) and by the French Agence Nationale de Recherche (ANR T-ERC-CoG grant ANR-23-ERCC-0007-01 to S.V.L.). Finally, this project benefited from MNHN Transhumance support, Origin and Evolution department of the MNHN, M-FED 2021 and CNRS-INSU Tellus fundings.

References

Alexander, B.W., Bau, M., Andersson, P., Dulski, P., 2008. Continentally-derived solutes in shallow Archean seawater: rare earth element and Nd isotope evidence in iron formation from the 2.9Ga Pongola Supergroup, South Africa. Geochim. Cosmochim. Acta 72, 378–394. https://doi.org/10.1016/j.gca.2007.10.028.

Allwood, A.C., Walter, M.R., Kamber, B.S., Marshall, C.P., Burch, I.W., 2006. Stromatolite reef from the early Archaean era of Australia. Nature 441, 714–718. https://doi.org/10.1038/nature04764.

Allwood, A.C., Kamber, B.S., Walter, M.R., Burch, I.W., Kanik, I., 2010. Trace elements record depositional history of an early Archean stromatolitic carbonate platform. Chem. Geol. 270, 148–163. https://doi.org/10.1016/j.chemgeo.2009.11.013.

Allwood, A.C., Burch, I.W., Rouchy, J.M., Coleman, M., 2013. Morphological Biosignatures in Gypsum: Diverse Formation Processes of Messinian (~6.0 Ma) Gypsum Stromatolites. Astrobiology 13, 870–886. https://doi.org/10.1089/ast.2013.1021.

Allwood, A.C., Rosing, M.T., Flannery, D.T., Hurowitz, J.A., Heirwegh, C.M., 2018. Reassessing evidence of life in 3,700-million-year-old rocks of Greenland. Nature 563, 241–244. https://doi.org/10.1038/s41586-018-0610-4.

Aloisi, G., 2008. The calcium carbonate saturation state in cyanobacterial mats throughout Earth's history. Geochim. Cosmochim. Acta 72, 6037–6060. https://doi.org/10.1016/j.gca.2008.10.007.

Álvaro, J.J., Macouin, M., Bauluz, B., Clausen, S., Ader, M., 2007. The Ediacaran sedimentary architecture and carbonate productivity in the Atar cliffs, Adrar, Mauritania: Palaeoenvironments, chemostratigraphy and diagenesis. Precambrian Res. 153, 236–261. https://doi.org/10.1016/j.precamres.2006.11.010.

Anbar, A.D., Duan, Y., Lyons, T.W., Arnold, G.L., Kendall, B., Creaser, R.A., Kaufman, A. J., Gordon, G.W., Scott, C., Garvin, J., Buick, R., 2007. A Whiff of Oxygen before the Great Oxidation Event? Science 317, 1903–1906. https://doi.org/10.1126/science.1140325.

Anderson, R.F., Fleisher, M.Q., LeHuray, A.P., 1989. Concentration, oxidation state, and particulate flux of uranium in the Black Sea. Geochim. Cosmochim. Acta 53, 2215–2224. https://doi.org/10.1016/0016-7037(89)90345-1.

Aretz, M., Chevaliers, E., 2007. After the collapse of stromatoporid-coral reefs — the Famennian and Dinantian reefs of Belgium: much more than Waulsortian mounds. Geol. Soc. Lond. Spec. Publ. 275, 163–188. https://doi.org/10.1144/GSL.SP.2007.275.01.11.

Armienta, M.A., Vilaclara, G., De la Cruz-Reyna, S., Ramos, S., Ceniceros, N., Cruz, O., Aguayo, A., Arcega-Cabrera, F., 2008. Water chemistry of lakes related to active and inactive Mexican volcanoes. J. Volcanol. Geotherm. Res. Volcan. Lakes Environ. Impact. Volcan. Fluid. 178, 249–258. https://doi.org/10.1016/j.jvolgeores.2008.06.019.

Arnold, G.L., Anbar, A.D., Barling, J., Lyons, T.W., 2004. Molybdenum Isotope evidence for Widespread Anoxia in Mid-Proterozoic Oceans. Science 304, 87–90. https://doi.org/10.1126/science.1091785.

Arp, G., Ostertag-Henning, C., Yücekent, S., Reitner, J., Thiel, V., 2008. Methane-related microbial gypsum calcitization in stromatolites of a marine evaporative setting (Münder Formation, Upper Jurassic, Hils Syncline, North Germany). Sedimentology 55, 1227–1251. https://doi.org/10.1111/j.1365-3091.2007.00944.x.

Awramik, S.M., 1992. The History and Significance of Stromatolites. Early Org. Evol. 435–449.

Awramik, S.M., Grey, K., 2005. Stromatolites: biogenicity, biosignatures, and bioconfusion. Astrobiol. Planet. Mission. 5906, 227–235. https://doi.org/10.1117/12.625556.

Awramik, S., Margulis, L., 1974. Definition of Stromatolite: Stromatolite Newsletter (Unpublished), v. 2.

Awramik, S.M., Sprinkle, J., 1999. Proterozoic stromatolites: the first marine evolutionary biota. Hist. Biol. 13, 241–253. https://doi.org/10.1080/08912969909386584.

Awramik, S.M., Vanyo, J.P., 1986. Heliotropism in Modern Stromatolites. Science 231, 1279–1281. https://doi.org/10.1126/science.231.4743.1279.

Awramik, S.M., Margulis, L., Barghoorn, E.S., 1976. Chapter 4.4 Evolutionary Processes in the Formation of Stromatolites. Develop. Sedimentol., Stromat. 20, 149–162. https://doi.org/10.1016/S0070-4571(08)71135-X.

Baker, P.A., Gieskes, J.M., Elderfield, H., 1982. Diagenesis of carbonates in deep-sea sediments; evidence from Sr/ca ratios and interstitial dissolved Sr (super 2+) data. J. Sediment. Res. 52, 71–82. https://doi.org/10.1306/212F7EE1-2B24-11D7-8648000102C1865D.

Barrat, J.-A., Bayon, G., Lalonde, S., 2023. Calculation of cerium and lanthanum anomalies in geological and environmental samples. Chem. Geol. 615, 121202 https://doi.org/10.1016/j.chemgeo.2022.121202.

Bartley, J.K., Kah, L.C., Frank, T.D., Lyons, T.W., 2015. Deep-water microbialites of the Mesoproterozoic dismal Lakes Group: microbial growth, lithification, and implications for coniform stromatolites. Geobiology 13, 15–32. https://doi.org/10.1111/gbi.12114.

Battistuzzi, F.U., Feijao, A., Hedges, S.B., 2004. A genomic timescale of prokaryote evolution: insights into the origin of methanogenesis, phototrophy, and the colonization of land. BMC Evol. Biol. 4, 44. https://doi.org/10.1186/1471-2148-4-44.

Bau, M., 1991. Rare-earth element mobility during hydrothermal and metamorphic fluid-rock interaction and the significance of the oxidation state of europium. Chem. Geol. 93, 219–230. https://doi.org/10.1016/0009-2541(91)90115-8.

Bau, M., 1993. Effects of syn- and post-depositional processes on the rare-earth element distribution in Precambrian iron-formations. ejm 5, 257–268. https://doi.org/10.1127/ejm/5/2/0257.

Bau, M., Dulski, P., 1996a. Distribution of yttrium and rare-earth elements in the Penge and Kuruman iron-formations, Transvaal Supergroup, South Africa. Precambrian Res. Geol. Geochem. Transvaal Supergroup 79, 37–55. https://doi.org/10.1016/0301-9268(95)00087-9.

Bau, M., Dulski, P., 1996b. Anthropogenic origin of positive gadolinium anomalies in river waters. Earth Planet. Sci. Lett. 143, 245–255. https://doi.org/10.1016/0012-821X(96)00127-6.

Bau, M., Dulski, P., Möller, P., 1995. Yttrium and Holmium in South Pacific Seawater: Vertical Distribution and Possible Fractionation Mechanisms.
Bau, M., Balan, S., Schmidt, K., Koschinsky, A., 2010. Rare earth elements in mussel shells of the Mytilidae family as tracers for hidden and fossil high-temperature hydrothermal systems. Earth Planet. Sci. Lett. 299, 310–316. https://doi.org/10.1016/j.epsl.2010.09.011.
Bekker, A., Karhu, J.A., Eriksson, K.A., Kaufman, A.J., 2003. Chemostratigraphy of Paleoproterozoic carbonate successions of the Wyoming Craton: tectonic forcing of biogeochemical change? Precambrian Res. 120, 279–325. https://doi.org/10.1016/S0301-9268(02)00164-X.
Berner, R.A., 1999. A New look at the long-term Carbon Cycle. GSA Today 9, 1–6.
Bertrand-Sarfati, J., Monty, C., 2012. Phanerozoic stromatolites II. Springer Science & Business Media.
Bertrand-Sarfati, J., Flicoteaux, R., Moussine-Pouchkine, A., Ait Kaci, A.A., 1997. Lower Cambrian apatitic stromatolites and phosphatenites related to the glacio-eustatic cratonic rebound (Sahara, Algeria). J. Sediment. Res. 67, 957–974. https://doi.org/10.1306/D426868A-2B26-11D7-8648000102C1865D.
Birgel, D., Meister, P., Lundberg, R., Horath, T.D., Bontognali, T.R.R., Bahniuk, A.M., de Rezende, C.E., Vasconcelos, C., McKenzie, J.A., 2015. Methanogenesis produces strong 13C enrichment in stromatolites of Lagoa Salgada, Brazil: a modern analogue for Palaeo-/Neoproterozoic stromatolites? Geobiology 13, 245–266. https://doi.org/10.1111/gbi.12130.
Bolhar, R., Van Kranendonk, M.J., 2007. A non-marine depositional setting for the northern Fortescue Group, Pilbara Craton, inferred from trace element geochemistry of stromatolitic carbonates. Precambrian Res. 155, 229–250. https://doi.org/10.1016/j.precamres.2007.02.002.
Bolhar, R., Kamber, B.S., Moorbath, S., Fedo, C.M., Whitehouse, M.J., 2004. Characterisation of early Archaean chemical sediments by trace element signatures. Earth Planet. Sci. Lett. 222, 43–60. https://doi.org/10.1016/j.epsl.2004.02.016.
Bolhar, R., Kamber, B.S., Moorbath, S., Whitehouse, M.J., Collerson, K.D., 2005. Chemical characterization of earth's most ancient clastic metasediments from the Isua Greenstone Belt, southern West Greenland. Geochim. Cosmochim. Acta 69, 1555–1573. https://doi.org/10.1016/j.gca.2004.09.023.
Bonilla-Rosso, G., Peimbert, M., Alcaraz, L.D., Hernández, I., Eguiarte, L.E., Olmedo-Alvarez, G., Souza, V., 2012. Comparative Metagenomics of two Microbial Mats at Cuatro Ciénegas Basin II: Community Structure and Composition in Oligotrophic Environments. Astrobiology 12, 659–673. https://doi.org/10.1089/ast.2011.0724.
Bonnand, P., Lalonde, S.V., Boyet, M., Heubeck, C., Homann, M., Nonnotte, P., Foster, I., Konhauser, K.O., Köhler, I., 2020. Post-depositional REE mobility in a Paleoarchean banded iron formation revealed by La-Ce geochronology: a cautionary tale for signals of ancient oxygenation. Earth Planet. Sci. Lett. 547, 116452 https://doi.org/10.1016/j.epsl.2020.116452.
Bosak, T., Liang, B., Sim, M.S., Petroff, A.P., 2009. Morphological record of oxygenic photosynthesis in conical stromatolites. Proc. Natl. Acad. Sci. 106, 10939–10943. https://doi.org/10.1073/pnas.0900885106.
Breit, G.N., Wanty, R.B., 1991. Vanadium accumulation in carbonaceous rocks: a review of geochemical controls during deposition and diagenesis. Chem. Geol. Trace Metal. Petrol. Geochem. 91, 83–97. https://doi.org/10.1016/0009-2541(91)90083-4.
Brigmon, R.L., Morris, P., Smith, G., 2008. Evaporite Microbial Films, Mats, Microbialites and Stromatolites. In: Dilek, Y., Furnes, H., Muehlenbachs, K. (Eds.), Links between Geological Processes, Microbial Activities&Evolution of Life: Microbes and Geology. Springer, Netherlands, Dordrecht, pp. 197–235. https://doi.org/10.1007/978-1-4020-8306-8_7.
Bristow, T.F., Kennedy, M.J., 2008. Carbon isotope excursions and the oxidant budget of the Ediacaran atmosphere and ocean. Geology 36, 863–866. https://doi.org/10.1130/G24968A.1.
Brock, T.D., 1978. Thermophilic Microorganisms and Life at High Temperatures, Springer Series in Microbiology. Springer, New York, New York, NY. https://doi.org/10.1007/978-1-4612-6284-8.
Bruckschen, P., Oesmann, S., Veizer, J., 1999. Isotope stratigraphy of the European Carboniferous: proxy signals for ocean chemistry, climate and tectonics. Chem. Geol. 161, 127–163. https://doi.org/10.1016/S0009-2541(99)00084-4.
Byrne, R.H., Kim, K.-H., 1990. Rare earth element scavenging in seawater. Geochim. Cosmochim. Acta 54, 2645–2656. https://doi.org/10.1016/0016-7037(90)90002-3.
Byrne, R.H., Lee, J.H., 1993. Comparative yttrium and rare earth element chemistries in seawater. In: Marine Chemistry, Marine Physical Chemistry - in memory of the Contributions Made to the Field by Dr. Ricardo Pytkowicz, 44, pp. 121–130. https://doi.org/10.1016/0304-4203(93)90197-V.
Cadeau, P., Jézéquel, D., Leboulanger, C., Fouilland, E., Le Floc'h, E., Chaduteau, C., Milesi, V., Guélard, J., Sarazin, G., Katz, A., d'Amore, S., Bernard, C., Ader, M., 2020. Carbon isotope evidence for large methane emissions to the Proterozoic atmosphere. Sci. Rep. 10, 18186. https://doi.org/10.1038/s41598-020-75100-x.
Calvert, S.E., Pedersen, T.F., 1993. Geochemistry of recent oxic and anoxic marine sediments: Implications for the geological record. In: Marine Geology, Marine Sediments, Burial, Pore Water Chemistry, Microbiology and Diagenesis, 113, pp. 67–88. https://doi.org/10.1016/0025-3227(93)90150-T.
Calvert, S.E., Pedersen, T.F., 2007. Chapter fourteen elemental proxies for palaeoclimatic and palaeoceanographic variability in marine sediments: interpretation and application. In: Hillaire-Marcel, C., De Vernal, A. (Eds.), Developments in Marine Geology, Proxies in Late Cenozoic Paleoceanography. Elsevier, pp. 567–644. https://doi.org/10.1016/S1572-5480(07)01019-6.
Cartigny, P., 2005. Stable Isotopes and the Origin of Diamond. Elements 1, 79–84. https://doi.org/10.2113/gselements.1.2.79.
Chafetz, H.S., Buczynski, C., 1992. Bacterially Induced Lithification of Microbial Mats. PALAIOS 7, 277–293. https://doi.org/10.2307/3514973.
Cherniak, D.J., 1998. REE diffusion in calcite. Earth Planet. Sci. Lett. 160, 273–287. https://doi.org/10.1016/S0012-821X(98)00087-9.
Cloud, P., 1973. Paleoecological significance of the banded iron-formation. Econ. Geol. 68, 1135–1143.
Cohen, A.S., Talbot, M.R., Awramik, S.M., Dettman, D.L., Abell, P., 1997. Lake level and paleoenvironmental history of Lake Tanganyika, Africa, as inferred from late Holocene and modern stromatolites. Geol. Soc. Am. Bull. 109 (4), 444–460.
D'Amelio, E.D., Des Marais, D.J., Cohen, J., 1989. Comparative Functional Ultrastructure of Two Hypersaline Submerged Cyanobacterial Mats - Guerrero Negro, Baja California Sur, Mexico, and Solar Lake, Sinai, Egypt.
Davison, W., 1993. Iron and manganese in lakes. Earth Sci. Rev. 34, 119–163. https://doi.org/10.1016/0012-8252(93)90029-7.
de Wet, C.B., Davis, K., 2010. Preservation potential of microorganism morphologies in tufas, sinters, and travertines through geologic time. Palaeobio Palaeoenv. 90, 139–152. https://doi.org/10.1007/s12549-010-0027-z.
Decho, A.W., Visscher, P.T., Reid, R.P., 2005. Production and cycling of natural microbial exopolymers (EPS) within a marine stromatolite. In: Noffke, N. (Ed.), Geobiology: Objectives, Concepts, Perspectives. Elsevier, Amsterdam, pp. 71–86. https://doi.org/10.1016/B978-0-444-52019-7.50008-5.
Degens, E.T., Epstein, S., 1962. Relationship between O18/O16 Ratios in Coexisting Carbonates, Cherts, and Diatomites1: Geological Notes. AAPG Bull. 46, 534–542. https://doi.org/10.1306/BC743841-16BE-11D7-8645000102C1865D.
Deynoux, M., Affaton, P., Trompette, R., Villeneuve, M., 2006. Pan-African tectonic evolution and glacial events registered in Neoproterozoic to Cambrian cratonic and foreland basins of West Africa. J. Afr. Earth Sci. 46, 397–426. https://doi.org/10.1016/j.jafrearsci.2006.08.005.
Ditchfield, P., Marshall, J.D., 1989. Isotopic variation in rhythmically bedded chalks: Paleotemperature variation in the Upper cretaceous. Geology 17, 842–845. https://doi.org/10.1130/0091-7613(1989)017<0842:IVIRBC>2.3.CO;2.
Dong, H., Huang, L., Zhao, L., Zeng, Q., Liu, X., Sheng, Y., Shi, L., Wu, G., Jiang, H., Li, F., Zhang, L., Guo, D., Li, G., Hou, W., Chen, H., 2022. A critical review of mineral–microbe interaction and co-evolution: mechanisms and applications. Natl. Sci. Rev. 9, nwac128 https://doi.org/10.1093/nsr/nwac128.
Dunk, R.M., Mills, R.A., Jenkins, W.J., 2002. A reevaluation of the oceanic uranium budget for the Holocene. In: Chemical Geology, Geochemistry of Crustal Fluids-Fluids in the Crust and Chemical Fluxes at the Earth's Surface, 190, pp. 45–67. https://doi.org/10.1016/S0009-2541(02)00110-9.
Dupraz, C., Visscher, P.T., 2005. Microbial lithification in marine stromatolites and hypersaline mats. Trends Microbiol. 13, 429–438. https://doi.org/10.1016/j.tim.2005.07.008.
Dupraz, C., Reid, R.P., Braissant, O., Decho, A.W., Norman, R.S., Visscher, P.T., 2009. Processes of carbonate precipitation in modern microbial mats. In: Earth-Science Reviews, Microbial Mats in Earth's Fossil Record of Life: Geobiology, 96, pp. 141–162. https://doi.org/10.1016/j.earscirev.2008.10.005.
Ejarque, E., Scholz, K., Wohlfahrt, G., Battin, T.J., Kainz, M.J., Schelker, J., 2021. Hydrology controls the carbon mass balance of a mountain lake in the eastern European Alps. Limnol. Oceanogr. 66, 2110–2125. https://doi.org/10.1002/lno.11712.
Epstein, S., Buchsbaum, R., Lowenstam, H., Urey, H.C., 1951. Carbonate-water isotopic temperature scale. GSA Bull. 62, 417–426. https://doi.org/10.1130/0016-7606(1951)62[417:CITS]2.0.CO;2.
Ernst, D.M., Bau, M., 2021. Banded iron formation from Antarctica: the 2.5 Ga old Mt. Ruker BIF and the antiquity of lanthanide tetrad effect and super-chondritic Y/Ho ratio in seawater. Gondwana Res. 91, 97–111. https://doi.org/10.1016/j.gr.2020.11.011.
Fantle, M.S., Maher, K.M., DePaolo, D.J., 2010. Isotopic approaches for quantifying the rates of marine burial diagenesis. Rev. Geophys. 48 https://doi.org/10.1029/2009RG000306.
Fantle, M.S., Barnes, B.D., Lau, K.V., 2020. The Role of Diagenesis in Shaping the Geochemistry of the Marine Carbonate Record. Annu. Rev. Earth Planet. Sci. 48, 549–583. https://doi.org/10.1146/annurev-earth-073019-060021.
Farías, M.E., Rascovan, N., Toneatti, D.M., Albarracín, V.H., Flores, M.R., Poiré, D.G., Collavino, M.M., Aguilar, O.M., Vazquez, M.P., Polerecky, L., 2013. The Discovery of Stromatolites developing at 3570 m above Sea Level in a High-Altitude Volcanic Lake Socompa, Argentinean Andes. PLoS One 8, e53497. https://doi.org/10.1371/journal.pone.0053497.
Fike, D.A., Grotzinger, J.P., Pratt, L.M., Summons, R.E., 2006. Oxidation of the Ediacaran Ocean. Nature 444, 744–747. https://doi.org/10.1038/nature05345.
Fogret, L., Sansjofre, P., Lalonde, S.V., 2024. Geochemical Dataset Associated with the National Museum of Natural History Microbialite Collection, Paris, Version 1.0. Interdisciplinary Earth Data Alliance (IEDA). https://doi.org/10.60520/IEDA/113109. Accessed 2024-04-17.
Foster, J.S., Green, S.J., 2011. Microbial Diversity in Modern Stromatolites. In: Tewari, V., Seckbach, J. (Eds.), STROMATOLITES: Interaction of Microbes with Sediments, Cellular Origin, Life in Extreme Habitats and Astrobiology. Springer Netherlands, Dordrecht, pp. 383–405. https://doi.org/10.1007/978-94-007-0397-1_17.
Galili, N., Shemesh, A., Yam, R., Brailovsky, I., Sela-Adler, M., Schuster, E.M., Collom, C., Bekker, A., Planavsky, N., Macdonald, F.A., Préat, A., Rudmin, M., Trela, W., Sturesson, U., Heikoop, J.M., Aurell, M., Ramajo, J., Halevy, I., 2019. The geologic history of seawater oxygen isotopes from marine iron oxides. Science 365, 469–473. https://doi.org/10.1126/science.aaw9247.
García Ruiz, J.M., Carnerup, A., Christy, A.G., Welham, N.J., Hyde, S.T., 2002. Morphology: an Ambiguous Indicator of Biogenicity. Astrobiology 2, 353–369. https://doi.org/10.1089/153110702762027925.

Gieskes, J.M., Kastner, M., Warner, T.B., 1975. Evidence for extensive diagenesis, Madagascar Basin, Deep Sea Drilling Site 245. Geochim. Cosmochim. Acta 39, 1385–1393. https://doi.org/10.1016/0016-7037(75)90117-9.
Gischler, E., Gibson, M.A., Oschmann, W., 2008. Giant Holocene Freshwater Microbialites, Laguna Bacalar, Quintana Roo, Mexico. Sedimentology 55, 1293–1309. https://doi.org/10.1111/j.1365-3091.2007.00946.x.
Golubic, S., 1976. Chapter 4.1 Organisms that Build Stromatolites. In: Walter, M.R. (Ed.), Developments in Sedimentology. Elsevier, Stromatolites, pp. 113–126. https://doi.org/10.1016/S0070-4571(08)71132-4.
Gong, J., Munoz-Saez, C., Wilmeth, D.T., Myers, K.D., Homann, M., Arp, G., Skok, J.R., van Zuilen, M.A., 2022. Morphogenesis of digitate structures in hot spring silica sinters of the El Tatio geothermal field, Chile. Geobiology 20, 137–155. https://doi.org/10.1111/gbi.12471.
Grandstaff, D.E., 1976. A kinetic study of the dissolution of uraninite. Econ. Geol. 71, 1493–1506. https://doi.org/10.2113/gsecongeo.71.8.1493.
Grey, K., Awramik, S.M., 2020. Handbook for the Study and Description of Microbialites. Geological Survey of Western Australia.
Grotzinger, J.P., Knoll, A.H., 1999. Stromatolites in Precambrian carbonates: Evolutionary Mileposts or Environmental Dipsticks? Annu. Rev. Earth Planet. Sci. 27, 313–358. https://doi.org/10.1146/annurev.earth.27.1.313.
Halverson, G.P., Wade, B.P., Hurtgen, M.T., Barovich, K.M., 2010. Neoproterozoic chemostratigraphy. In: Precambrian Research, Precambrian Isotope Stratigraphy, 182, pp. 337–350. https://doi.org/10.1016/j.precamres.2010.04.007.
Havas, R., Thomazo, C., Iniesto, M., Jézéquel, D., Moreira, D., Tavera, R., Caumartin, J., Muller, E., López-García, P., Benzerara, K., 2023. Biogeochemical processes captured by carbon isotopes in redox-stratified water columns: a comparative study of four modern stratified lakes along an alkalinity gradient. Biogeosciences 20, 2347–2367. https://doi.org/10.5194/bg-20-2347-2023.
Havig, J.R., Hamilton, T.L., Bachan, A., Kump, L.R., 2017. Sulfur and carbon isotopic evidence for metabolic pathway evolution and a four-stepped Earth system progression across the Archean and Paleoproterozoic. Earth Sci. Rev. 174, 1–21. https://doi.org/10.1016/j.earscirev.2017.06.014.
Hayes, J.M., Wedeking, K.W., Kaplan, I.R., 1983. Precambrian Organic Geochemistry - Preservation of the Record.
Hayes, J.M., Strauss, H., Kaufman, A.J., 1999. The abundance of 13C<math><msup><mi></mi><mn>13</mn></msup><mtext>C</mtext></math> in marine organic matter and isotopic fractionation in the global biogeochemical cycle of carbon during the past 800 Ma. Chem. Geol. 161, 103–125. https://doi.org/10.1016/S0009-2541(99)00083-2.
Helz, G.R., Miller, C.V., Charnock, J.M., Mosselmans, J.F.W., Pattrick, R.A.D., Garner, C. D., Vaughan, D.J., 1996. Mechanism of molybdenum removal from the sea and its concentration in black shales: EXAFS evidence. Geochim. Cosmochim. Acta 60, 3631–3642. https://doi.org/10.1016/0016-7037(96)00195-0.
Helz, G.R., Bura-Nakić, E., Mikac, N., Ciglenečki, I., 2011. New model for molybdenum behavior in euxinic waters. Chem. Geol. 284, 323–332. https://doi.org/10.1016/j.chemgeo.2011.03.012.
Hickman-Lewis, K., Cavalazzi, B., Foucher, F., Westall, F., 2018. Most ancient evidence for life in the Barberton greenstone belt: Microbial mats and biofabrics of the ~3.47 Ga Middle Marker horizon. Precambrian Res. 312, 45–67. https://doi.org/10.1016/j.precamres.2018.04.007.
Hodgskiss, M.S.W., Lalonde, S.V., Crockford, P.W., Hutchings, A.M., 2021. A carbonate molybdenum isotope and cerium anomaly record across the end-GOE: local records of global oxygenation. Geochim. Cosmochim. Acta 313, 313–339. https://doi.org/10.1016/j.gca.2021.08.013.
Hofmann, H.J., 2000. Archean Stromatolites as Microbial Archives. In: Riding, R.E., Awramik, S.M. (Eds.), Microbial Sediments. Springer, Berlin, Heidelberg, pp. 315–327. https://doi.org/10.1007/978-3-662-04036-2_34.
Hohl, S.V., Viehmann, S., 2021. Stromatolites as geochemical archives to reconstruct microbial habitats through deep time: potential and pitfalls of novel radiogenic and stable isotope systems. Earth Sci. Rev. 218, 103683 https://doi.org/10.1016/j.earscirev.2021.103683.
Holland, H.D., 1973. The Oceans; a possible source of Iron in Iron-Formations. Econ. Geol. 68, 1169–1172. https://doi.org/10.2113/gsecongeo.68.7.1169.
Holland, H.D., 1984. The Chemical Evolution of the Oceans and Atmosphere. Princeton University Press.
Holland, H.D., 2006. The oxygenation of the atmosphere and oceans. Philos. Trans. R. Soc. B 361, 903–915. https://doi.org/10.1098/rstb.2006.1838.
Hood, A.V.S., Planavsky, N.J., Wallace, M.W., Wang, X., 2018. The effects of diagenesis on geochemical paleoredox proxies in sedimentary carbonates. Geochim. Cosmochim. Acta 232, 265–287. https://doi.org/10.1016/j.gca.2018.04.022.
Hu, Z., Hohl, S.V., Viehmann, S., Meister, P., Tepe, N., 2023. No biological effect on magnesium isotope fractionation during stromatolite growth. Geochim. Cosmochim. Acta 358, 1–11. https://doi.org/10.1016/j.gca.2023.07.022.
Hummer, D.R., Golden, J.J., Hystad, G., Downs, R.T., Eleish, A., Liu, C., Ralph, J., Morrison, S.M., Meyer, M.B., Hazen, R.M., 2022. Evidence for the oxidation of Earth's crust from the evolution of manganese minerals. Nat. Commun. 13, 960. https://doi.org/10.1038/s41467-022-28589-x.
Husson, J.M., Peters, S.E., 2017. Atmospheric oxygenation driven by unsteady growth of the continental sedimentary reservoir. Earth Planet. Sci. Lett. 460, 68–75. https://doi.org/10.1016/j.epsl.2016.12.012.
Jaffrés, J.B.D., Shields, G.A., Wallmann, K., 2007. The oxygen isotope evolution of seawater: a critical review of a long-standing controversy and an improved geological water cycle model for the past 3.4 billion years. Earth Sci. Rev. 83, 83–122. https://doi.org/10.1016/j.earscirev.2007.04.002.
Jenkyns, H.C., Gale, A.S., Corfield, R.M., 1994. Carbon- and oxygen-isotope stratigraphy of the English Chalk and Italian Scaglia and its palaeoclimatic significance. Geol. Mag. 131, 1–34. https://doi.org/10.1017/S0016756800010451.
Jones, D.S., Brothers, R.W., Crüger Ahm, A.-S., Slater, N., Higgins, J.A., Fike, D.A., 2019. Sea level, carbonate mineralogy, and early diagenesis controlled δ13C records in Upper Ordovician carbonates. Geology 48, 194–199. https://doi.org/10.1130/G46861.1.
Kalkowsky, E., 1908. Oolith und Stromatolith im norddeutschen Buntsandstein. Z. Dtsch. Geol. Ges. 68–125.
Kamber, B.S., 2010. Archean mafic–ultramafic volcanic landmasses and their effect on ocean–atmosphere chemistry. Chem. Geol. 274, 19–28. https://doi.org/10.1016/j.chemgeo.2010.03.009.
Kamber, B.S., Greig, A., Collerson, K.D., 2005. A new estimate for the composition of weathered young upper continental crust from alluvial sediments, Queensland, Australia. Geochim. Cosmochim. Acta 69, 1041–1058. https://doi.org/10.1016/j.gca.2004.08.020.
Kamber, B.S., Webb, G.E., Gallagher, M., 2014. The rare earth element signal in Archaean microbial carbonate: information on ocean redox and biogenicity. J. Geol. Soc. Lond. 171, 745–763. https://doi.org/10.1144/jgs2013-110.
Kasting, J.F., Howard, M.T., Wallmann, K., Veizer, J., Shields, G., Jaffrés, J., 2006. Paleoclimates, ocean depth, and the oxygen isotopic composition of seawater. Earth Planet. Sci. Lett. 252, 82–93. https://doi.org/10.1016/j.epsl.2006.09.029.
Kaufman, A.J., Knoll, A.H., 1995. Neoproterozoic variations in the C-isotopic composition of seawater: stratigraphic and biogeochemical implications. In: Precambrian Research, Neoproterozoic Stratigraphy and Earth History, 73, pp. 27–49. https://doi.org/10.1016/0301-9268(94)00070-8.
Killingley, J.S., 1983. Seasonality Determination by Oxygen Isotopic Profile: A Reply to Bailey et al. Am. Antiq. 48, 399–403. https://doi.org/10.2307/280461.
Killingsworth, B.A., Sansjofre, P., Philippot, P., Cartigny, P., Thomazo, C., Lalonde, S.V., 2019. Constraining the rise of oxygen with oxygen isotopes. Nat. Commun. 10, 4924. https://doi.org/10.1038/s41467-019-12883-2.
Kim, K.-H., Byrne, R.H., Lee, J.H., 1991. Gadolinium behavior in seawater: a molecular basis for gadolinium anomalies. In: Marine Chemistry, Reactivity of Chemical Species in Aquatic Environments, 36, pp. 107–120. https://doi.org/10.1016/S0304-4203(09)90057-3.
Kipp, M.A., Krissansen-Totton, J., Catling, D.C., 2021. High Organic Burial Efficiency is Required to Explain Mass Balance in Earth's early Carbon Cycle. Glob. Biogeochem. Cycles 35. https://doi.org/10.1029/2020GB006707.
Knauth, L.P., 2005. Temperature and salinity history of the Precambrian Ocean: Implications for the course of microbial evolution. In: Noffke, N. (Ed.), Geobiology: Objectives, Concepts, Perspectives. Elsevier, Amsterdam, pp. 53–69. https://doi.org/10.1016/B978-0-444-52019-7.50007-3.
Knauth, L.P., Kennedy, M.J., 2009. The late Precambrian greening of the Earth. Nature 460, 728–732. https://doi.org/10.1038/nature08213.
Knoll, A.H., 2003. Biomineralization and Evolutionary history. Rev. Mineral. Geochem. 54, 329–356. https://doi.org/10.2113/0540329.
Knoll, A.H., Semikhatov, M.A., 1998. The genesis and time distribution of two distinctive Proterozoic stromatolite microstructures. PALAIOS 13, 408–422. https://doi.org/10.2307/3515471.
Kreitsmann, T., Bau, M., 2023. Rare earth elements in alkaline Lake Neusiedl, Austria, and the use of gadolinium microcontamination as water source tracer. Appl. Geochem. 159, 105792 https://doi.org/10.1016/j.apgeochem.2023.105792.
Lalonde, S.V., Konhauser, K.O., 2015. Benthic perspective on Earth's oldest evidence for oxygenic photosynthesis. Proc. Natl. Acad. Sci. 112, 995–1000. https://doi.org/10.1073/pnas.1415718112.
Lalonde, S.V., Rigoussen, D., Fogret, L., Sansjofre, P., 2024. Compilation of major and trace element geochemical data from literature for sedimentary carbonates worldwide. In: Interdisciplinary Earth Data Alliance (IEDA).
Last, F.M., Last, W.M., Fayek, M., Halden, N.M., 2013. Occurrence and significance of a cold-water carbonate pseudomorph in microbialites from a saline lake. J. Paleolimnol. 50, 505–517. https://doi.org/10.1007/s10933-013-9742-6.
Lau, K.V., Hardisty, D.S., 2022. Modeling the impacts of diagenesis on carbonate paleoredox proxies. Geochim. Cosmochim. Acta 337, 123–139. https://doi.org/10.1016/j.gca.2022.09.021.
Lawrence, M.G., Kamber, B.S., 2006. The behaviour of the rare earth elements during estuarine mixing—revisited. Mar. Chem. 100, 147–161. https://doi.org/10.1016/j.marchem.2005.11.007.
Lawrence, M.G., Greig, A., Collerson, K.D., Kamber, B.S., 2006. Rare Earth Element and Yttrium Variability in South East Queensland Waterways. Aquat. Geochem. 12, 39–72. https://doi.org/10.1007/s10498-005-4471-8.
Liu, X.-M., Hardisty, D.S., Lyons, T.W., Swart, P.K., 2019. Evaluating the fidelity of the cerium paleoredox tracer during variable carbonate diagenesis on the Great Bahamas Bank. Geochim. Cosmochim. Acta 248, 25–42. https://doi.org/10.1016/j.gca.2018.12.028.
Logan, B.W., 1961. Cryptozoon and Associate Stromatolites from the recent, Shark Bay, Western Australia. J. Geol. 69, 517–533. https://doi.org/10.1086/626769.
Lyons, T.W., Reinhard, C.T., Planavsky, N.J., 2014. The rise of oxygen in Earth's early ocean and atmosphere. Nature 506, 307–315. https://doi.org/10.1038/nature13068.
Macalady, J.L., Dattagupta, S., Schaperdoth, I., Jones, D.S., Druschel, G.K., Eastman, D., 2008. Niche differentiation among sulfur-oxidizing bacterial populations in cave waters. ISME J. 2, 590–601. https://doi.org/10.1038/ismej.2008.25.
Maynard, J.B., 2010. The Chemistry of Manganese Ores through Time: a Signal of increasing Diversity of Earth-Surface Environments. Econ. Geol. 105, 535–552. https://doi.org/10.2113/gsecongeo.105.3.535.

Mcloughlin, N., Wilson, L.A., Brasier, M.D., 2008. Growth of synthetic stromatolites and wrinkle structures in the absence of microbes – implications for the early fossil record. Geobiology 6, 95–105. https://doi.org/10.1111/j.1472-4669.2007.00141.x.

McManus, J., Nägler, T.F., Siebert, C., Wheat, C.G., Hammond, D.E., 2002. Oceanic molybdenum isotope fractionation: Diagenesis and hydrothermal ridge-flank alteration. Geochem. Geophys. Geosyst. 3, 1–9. https://doi.org/10.1029/2002GC000356.

Melezhik, V.A., Fallick, A.E., 1996. A widespread positive δ13Ccarb anomaly at around 2.33–2.06 Ga on the Fennoscandian Shield: a paradox? Terra Nova 8, 141–157.

Melezhik, V.A., Fallick, A.E., 2003. δ13C and δ18O variations in primary and secondary carbonate phases: several contrasting examples from Palaeoproterozoic 13C-rich metamorphosed dolostones. Chem. Geol. 201, 213–228. https://doi.org/10.1016/j.chemgeo.2003.07.003.

Merschel, G., Bau, M., Dantas, E.L., 2017. Contrasting impact of organic and inorganic nanoparticles and colloids on the behavior of particle-reactive elements in tropical estuaries: an experimental study. Geochim. Cosmochim. Acta 197, 1–13. https://doi.org/10.1016/j.gca.2016.09.041.

Mojzsis, S.J., Harrison, T.M., Pidgeon, R.T., 2001. Oxygen-isotope evidence from ancient zircons for liquid water at the Earth's surface 4,300 Myr ago. Nature 409, 178–181. https://doi.org/10.1038/35051557.

Monty, C., 1974. Precambrian background and Phanerozoic history of stromatolitic communities, an overview. Ann. Soc. Geol. Belg.

Morais, L., Fairchild, T.R., Freitas, B.T., Rudnitzki, I.D., Silva, E.P., Lahr, D., Moreira, A. C., Abrahão Filho, E.A., Leme, J.M., Trindade, R.I.F., 2021. Doushantuo-Pertatataka—like Acritarchs from the late Ediacaran Bocaina Formation (Corumbá Group, Brazil). Front. Earth Sci. 9 https://doi.org/10.3389/feart.2021.787011.

Muehlenbachs, K., Clayton, R.N., 1976. Oxygen isotope composition of the oceanic crust and its bearing on seawater. J. Geophys. Res. 1896-1977 (81), 4365–4369. https://doi.org/10.1029/JB081i023p04365.

Noffke, N., 2009. The criteria for the biogeneicity of microbially induced sedimentary structures (MISS) in Archean and younger, sandy deposits. In: Earth-Science Reviews, Microbial Mats in Earth's Fossil Record of Life: Geobiology, 96, pp. 173–180. https://doi.org/10.1016/j.earscirev.2008.08.002.

Nozaki, Y., 2001. Rare Earth elements and their Isotopes in the Ocean. In: Encyclopedia of Ocean Sciences. Elsevier, pp. 2354–2366. https://doi.org/10.1006/rwos.2001.0284.

Nozaki, Y., Zhang, J., Amakawa, H., 1997. The fractionation between Y and Ho in the marine environment. Earth Planet. Sci. Lett. 148, 329–340. https://doi.org/10.1016/S0012-821X(97)00034-4.

Nutman, A.P., Bennett, V.C., Friend, C.R.L., Van Kranendonk, M.J., Chivas, A.R., 2016. Rapid emergence of life shown by discovery of 3,700-million-year-old microbial structures. Nature 537, 535–538. https://doi.org/10.1038/nature19355.

Nutman, A.P., Friend, C.R.L., Bennett, V.C., Van Kranendonk, M., Chivas, A.R., 2019. Reconstruction of a 3700 Ma transgressive marine environment from Isua (Greenland): Sedimentology, stratigraphy and geochemical signatures. Lithos 346–347, 105164. https://doi.org/10.1016/j.lithos.2019.105164.

Nutman, A.P., Bennett, V.C., Friend, C.R.L., Van Kranendonk, M.J., 2021. In support of rare relict ~3700 Ma stromatolites from Isua (Greenland). Earth Planet. Sci. Lett. 562, 116850 https://doi.org/10.1016/j.epsl.2021.116850.

Ojakangas, G.W., Awramik, S.M., Storrie-Lombardi, M.C., 2023. Stromatolite photomorphogenesis: lighting up their shape. Int. J. Astrobiol. 22, 33–56. https://doi.org/10.1017/S1473550422000313.

Pacton, M., Hunger, G., Martinuzzi, V., Cusminsky, G., Burdin, B., Barmettler, K., Vasconcelos, C., Ariztegui, D., 2016. Organomineralization processes in freshwater stromatolites: a living example from eastern Patagonia. Depositional Rec. 1, 130–146. https://doi.org/10.1002/dep2.7.

Papineau, D., Walker, J.J., Mojzsis, S.J., Pace, N.R., 2005. Composition and Structure of Microbial Communities from Stromatolites of Hamelin Pool in Shark Bay, Western Australia. Appl. Environ. Microbiol. 71, 4822–4832. https://doi.org/10.1128/AEM.71.8.4822-4832.2005.

Partin, C.A., Bekker, A., Planavsky, N.J., Scott, C.T., Gill, B.C., Li, C., Podkovyrov, V., Maslov, A., Konhauser, K.O., Lalonde, S.V., Love, G.D., Poulton, S.W., Lyons, T.W., 2013a. Large-scale fluctuations in Precambrian atmospheric and oceanic oxygen levels from the record of U in shales. Earth Planet. Sci. Lett. 369–370, 284–293. https://doi.org/10.1016/j.epsl.2013.03.031.

Partin, C.A., Lalonde, S.V., Planavsky, N.J., Bekker, A., Rouxel, O.J., Lyons, T.W., Konhauser, K.O., 2013b. Uranium in iron formations and the rise of atmospheric oxygen. In: Chemical Geology, Special Issue Dedicated to H.D. Holland: Evolution of the Atmosphere and Ocean Through Time, 362, pp. 82–90. https://doi.org/10.1016/j.chemgeo.2013.09.005.

Patry, L.A., Bonnand, P., Boyet, M., Afroz, M., Wilmeth, D.T., Ramsay, B., Nonnotte, P., Homann, M., Sansjofre, P., Fralick, P.W., Lalonde, S.V., 2024. Trace element and Ce isotope data associated with the study of Patry et al. (2024; in revision). In: Interdisciplinary Earth Data Alliance (IEDA).

Peters, S.E., Husson, J.M., Wilcots, J., 2017. The rise and fall of stromatolites in shallow marine environments. Geology 45, 487–490. https://doi.org/10.1130/G38931.1.

Petrash, D.A., Lalonde, S.V., Pecoits, E., Gingras, M., Konhauser, K.O., 2010. Microbially Catalyzed Cementation of Modern Gypsum-Dominated Microbialites.

Petrash, D.A., Gingras, M.K., Lalonde, S.V., Orange, F., Pecoits, E., Konhauser, K.O., 2012. Dynamic controls on accretion and lithification of modern gypsum-dominated thrombolites, Los Roques, Venezuela. Sediment. Geol. 245–246, 29–47. https://doi.org/10.1016/j.sedgeo.2011.12.006.

Planavsky, N., Rouxel, O., Bekker, A., Shapiro, R., Fralick, P., Knudsen, A., 2009. Iron-oxidizing microbial ecosystems thrived in late Paleoproterozoic redox-stratified oceans. Earth Planet. Sci. Lett. 286, 230–242. https://doi.org/10.1016/j.epsl.2009.06.033.

Planavsky, N.J., Robbins, L.J., Kamber, B.S., Schoenberg, R., 2020. Weathering, alteration and reconstructing Earth's oxygenation. Interf. Focus 10, 20190140. https://doi.org/10.1098/rsfs.2019.0140.

Polgári, M., Gyollai, I., 2022. Comparative Study of Formation Conditions of Fe-Mn Ore Microbialites based on Mineral Assemblages: a critical Self-Overview. Minerals 12, 1273. https://doi.org/10.3390/min12101273.

Pope, M.C., Grotzinger, J.P., Schreiber, B.C., 2000. Evaporitic Subtidal Stromatolites Produced by in situ Precipitation: Textures, Facies Associations, and Temporal significance. J. Sediment. Res. 70, 1139–1151. https://doi.org/10.1306/062099701139.

Potts, P.J., Thompson, M., Kane, J.S., Webb, P.C., Carignan, J., 2002. GeoPT6 - An international proficiency test for analytical geochemistry laboratories - Report on round 6 (OU-3: Nanhoron microgranite) and 6A (CAL-S: CRPG limestone). Geostandards Newsletter 1–37.

Poulton, S.W., Canfield, D.E., 2011. Ferruginous Conditions: a Dominant Feature of the Ocean through Earth's history. Elements 7, 107–112. https://doi.org/10.2113/gselements.7.2.107.

Pratt, B.R., 2000. Microbial Contribution to Reefal Mud-Mounds in Ancient Deep-Water Settings: Evidence from the Cambrian 282–288. https://doi.org/10.1007/978-3-662-04036-2_30.

Prave, A.R., Kirsimäe, K., Lepland, A., Fallick, A.E., Kreitsmann, T., Deines, Yu.E., Romashkin, A.E., Rychanchik, D.V., Medvedev, P.V., Moussavou, M., Bakakas, K., Hodgskiss, M.S.W., 2021. The grandest of them all: the Lomagundi–Jatuli Event and Earth's oxygenation. J. Geol. Soc. Lond. 179 https://doi.org/10.1144/jgs2021-036 jgs2021-036.

Prokoph, A., Shields, G.A., Veizer, J., 2008. Compilation and time-series analysis of a marine carbonate δ18O, δ13C, 87Sr/86Sr and δ34S database through Earth history. Earth Sci. Rev. 87, 113–133. https://doi.org/10.1016/j.earscirev.2007.12.003.

Reitner, J., 1993. Modern cryptic microbialite/metazoan facies from Lizard Island (Great Barrier Reef, Australia) formation and concepts. Facies 29, 3–39. https://doi.org/10.1007/BF02536915.

Riding, R., 1992. Temporal variation in calcification in marine cyanobacteria. J. Geol. Soc. 149 (6), 979–989.

Riding, R., 2000. Microbial carbonates: the geological record of calcified bacterial–algal mats and biofilms. Sedimentology 47, 179–214. https://doi.org/10.1046/j.1365-3091.2000.00003.x.

Riding, R., 2006. Microbial carbonate abundance compared with fluctuations in metazoan diversity over geological time. In: Sedimentary Geology, Microbialites and Microbial Communities, 185, pp. 229–238. https://doi.org/10.1016/j.sedgeo.2005.12.015.

Riding, R., 2011. The Nature of Stromatolites: 3,500 Million Years of History and a Century of Research, Lecture Notes in Earth Sciences. Springer, Berlin, Heidelberg. https://doi.org/10.1007/978-3-642-10415-2_3.

Riding, R.E., Awramik, S.M., 2000. Microbial Sediments. Springer Science & Business Media.

Riding, R., Fralick, P., Liang, L., 2014. Identification of an Archean marine oxygen oasis. Precambrian Res. 251, 232–237. https://doi.org/10.1016/j.precamres.2014.06.017.

Rishworth, G.M., Perissinotto, R., Bird, M.S., 2016. Coexisting living stromatolites and infaunal metazoans. Oecologia 182, 539–545.

Rizzo, V., Farias, M.E., Cantasano, N., Billi, D., Contreras, M., Pontenani, F., Bianciardi, G., 2015. Structures/Textures of Living/Fossil Microbialites and their Implications in Biogenicity: An Astrobiological Point of View.

Robbins, L.J., Lalonde, S.V., Planavsky, N.J., Partin, C.A., Reinhard, C.T., Kendall, B., Scott, C., Hardisty, D.S., Gill, B.C., Alessi, D.S., Dupont, C.L., Saito, M.A., Crowe, S. A., Poulton, S.W., Bekker, A., Lyons, T.W., Konhauser, K.O., 2016. Trace elements at the intersection of marine biological and geochemical evolution. Earth Sci. Rev. 163, 323–348. https://doi.org/10.1016/j.earscirev.2016.10.013.

Robbins, L.J., Fakhraee, M., Smith, A.J.B., Bishop, B.A., Swanner, E.D., Peacock, C.L., Wang, C.-L., Planavsky, N.J., Reinhard, C.T., Crowe, S.A., Lyons, T.W., 2023. Manganese oxides, Earth surface oxygenation, and the rise of oxygenic photosynthesis. Earth Sci. Rev. 239, 104368 https://doi.org/10.1016/j.earscirev.2023.104368.

Romaniello, S.J., Herrmann, A.D., Anbar, A.D., 2016. Syndepositional diagenetic control of molybdenum isotope variations in carbonate sediments from the Bahamas. Chem. Geol. 438, 84–90. https://doi.org/10.1016/j.chemgeo.2016.05.019.

Rongemaille, E., Bayon, G., Pierre, C., Bollinger, C., Chu, N.C., Fouquet, Y., Riboulot, V., Voisset, M., 2011. Rare earth elements in cold seep carbonates from the Niger delta. Chem. Geol. 286, 196–206. https://doi.org/10.1016/j.chemgeo.2011.05.001.

Rudnick, R.L., Gao, S., 2003. 3.01 - Composition of the Continental Crust. In: Holland, H. D., Turekian, K.K. (Eds.), Treatise on Geochemistry. Pergamon, Oxford, pp. 1–64. https://doi.org/10.1016/B0-08-043751-6/03016-4.

Russell, A.D., Morford, J.L., 2001. The behavior of redox-sensitive metals across a laminated–massive–laminated transition in Saanich Inlet, British Columbia. Mar. Geol. 174, 341–354. https://doi.org/10.1016/S0025-3227(00)00159-6.

Sahoo, S.K., Planavsky, N.J., Kendall, B., Wang, X., Shi, X., Scott, C., Anbar, A.D., Lyons, T.W., Jiang, G., 2012. Ocean oxygenation in the wake of the Marinoan glaciation. Nature 489, 546–549. https://doi.org/10.1038/nature11445.

Salama, W., El Aref, M.M., Gaupp, R., 2013. Mineral evolution and processes of ferruginous microbialite accretion – an example from the Middle Eocene stromatolitic and ooidal ironstones of the Bahariya Depression, Western Desert, Egypt. Geobiology 11, 15–28. https://doi.org/10.1111/gbi.12011.

Santrock, Jeffrey, Studley, S.A., Hayes, J.M., 1985. Isotopic analyses based on the mass spectra of carbon dioxide. Anal. Chem. 57, 1444–1448. https://doi.org/10.1021/ac00284a060.

Sayles, F.L., Manheim, F.T., 1975. Interstitial solutions and diagenesis in deeply buried marine sediments: results from the Deep Sea Drilling Project. Geochim. Cosmochim. Acta 39, 103–127. https://doi.org/10.1016/0016-7037(75)90165-9.
Schidlowski, M., Eichmann, R., Junge, C.E., 1976. Carbon isotope geochemistry of the Precambrian Lomagundi carbonate province, Rhodesia. Geochim. Cosmochim. Acta 40, 449–455. https://doi.org/10.1016/0016-7037(76)90010-7.
Schidlowski, M., Matzigkeit, U., Krumbein, W.E., 1984. Superheavy organic carbon from hypersaline microbial mats. Naturwissenschaften 71, 303–308. https://doi.org/10.1007/BF00396613.
Schopf, J.W., 1983. Earth's Earliest Biosphere: Its Origin and Evolution. Princeton University Press, United States.
Schopf, J.W., Kudryavtsev, A.B., 2012. Biogenicity of Earth's earliest fossils: a resolution of the controversy. Gondwana Res. 22, 761–771. https://doi.org/10.1016/j.gr.2012.07.003.
Semikhatov, M.A., Gebelein, C.D., Cloud, P., Awramik, S.M., Benmore, W.C., 1979. Stromatolite morphogenesis—progress and problems. Can. J. Earth Sci. 16, 992–1015. https://doi.org/10.1139/e79-088.
Sforna, M.C., Philippot, P., Somogyi, A., van Zuilen, M.A., Medjoubi, K., Schoepp-Cothenet, B., Nitschke, W., Visscher, P.T., 2014. Evidence for arsenic metabolism and cycling by microorganisms 2.7 billion years ago. Nat. Geosci. 7, 811–815. https://doi.org/10.1038/ngeo2276.
Shapiro, R.S., 2007. CHAPTER 22 - Stromatolites: A 3.5-Billion-Year Ichnologic Record. In: Miller, W. (Ed.), Trace Fossils. Elsevier, Amsterdam, pp. 382–390. https://doi.org/10.1016/B978-044452949-7/50148-0.
Shields, G., Veizer, J., 2002. Precambrian marine carbonate isotope database: Version 1.1. Geochem. Geophys. Geosyst. 3 https://doi.org/10.1029/2001GC000266, 1 of 12–12 12.
Sturchio, N.C., Antonio, M.R., Soderholm, L., Sutton, S.R., Brannon, J.C., 1998. Tetravalent Uranium in Calcite. Science 281, 971–973. https://doi.org/10.1126/science.281.5379.971.
Sugitani, K., Lepot, K., Nagaoka, T., Mimura, K., Van Kranendonk, M., Oehler, D.Z., Walter, M.R., 2010. Biogenicity of Morphologically Diverse Carbonaceous Microstructures from the ca. 3400 Ma Strelley Pool Formation, in the Pilbara Craton, Western Australia. Astrobiology 10, 899–920. https://doi.org/10.1089/ast.2010.0513.
Sumner, D.Y., Hawes, I., Mackey, T.J., Jungblut, A.D., Doran, P.T., 2015. Antarctic microbial mats: a modern analog for Archean lacustrine oxygen oases. Geology 43, 887–890. https://doi.org/10.1130/G36966.1.
Swart, P.K., 2015. The geochemistry of carbonate diagenesis: the past, present and future. Sedimentology 62, 1233–1304. https://doi.org/10.1111/sed.12205.
Tan, Q., Shi, Z., Hu, X., Wang, Y., Tian, Y., Wang, C., 2018. Diagenesis of microbialites in the lower Cambrian Qingxudong Formation, South China: Implications for the origin of porosity in deep microbial carbonates. J. Nat. Gas Sci. Eng. 51, 166–182. https://doi.org/10.1016/j.jngse.2017.12.031.
Taylor, S.R., McLennan, S.M., 1985. The Continental Crust: Its Composition and Evolution.
Tepe, N., Bau, M., 2016. Behavior of rare earth elements and yttrium during simulation of arctic estuarine mixing between glacial-fed river waters and seawater and the impact of inorganic (nano-)particles. Chem. Geol. 438, 134–145. https://doi.org/10.1016/j.chemgeo.2016.06.001.
Thoby, M., Konhauser, K.O., Fralick, P.W., Altermann, W., Visscher, P.T., Lalonde, S.V., 2019. Global importance of oxic molybdenum sinks prior to 2.6 Ga revealed by the Mo isotope composition of Precambrian carbonates. Geology 47, 559–562. https://doi.org/10.1130/G45706.1.
Thomazo, C., Ader, M., Farquhar, J., Philippot, P., 2009. Methanotrophs regulated atmospheric sulfur isotope anomalies during the Mesoarchean (Tumbiana Formation, Western Australia). Earth Planet. Sci. Lett. 279, 65–75. https://doi.org/10.1016/j.epsl.2008.12.036.
Thomazo, C., Couradeau, E., Giraldo-Silva, A., Marin-Carbonne, J., Brayard, A., Homann, M., Sansjofre, P., Lalonde, S.V., Garcia-Pichel, F., 2020. Biological Soil Crusts as Modern Analogs for the Archean Continental Biosphere: Insights from Carbon and Nitrogen Isotopes. Astrobiology 20, 815–819. https://doi.org/10.1089/ast.2019.2144.
Tostevin, R., Shields, G.A., Tarbuck, G.M., He, T., Clarkson, M.O., Wood, R.A., 2016. Effective use of cerium anomalies as a redox proxy in carbonate-dominated marine settings. Chem. Geol. 438, 146–162. https://doi.org/10.1016/j.chemgeo.2016.06.027.
Tribovillard, N., Algeo, T.J., Lyons, T., Riboulleau, A., 2006. Trace metals as paleoredox and paleoproductivity proxies: an update. Chem. Geol. 232, 12–32. https://doi.org/10.1016/j.chemgeo.2006.02.012.
Urey, H.C., Lowenstam, H.A., Epstein, S., McKinney, C.R., 1951. Measurement of paleotemperatures and temperatures of the upper cretaceous of England, Denmark, and the Southeastern United States. GSA Bull. 62, 399–416. https://doi.org/10.1130/0016-7606(1951)62[399:MOPATO]2.0.CO;2.
Van Kranendonk, M.J., Philippot, P., Lepot, K., Bodorkos, S., Pirajno, F., 2008. Geological setting of Earth's oldest fossils in the ca. 3.5Ga Dresser Formation, Pilbara Craton, Western Australia. Precambrian Res. 167, 93–124. https://doi.org/10.1016/j.precamres.2008.07.003.
Veizer, J., 1983. Chapter 8. Trace Elements and Isotopes in Sedimentary Carbonates. De Gruyter, pp. 265–300. https://doi.org/10.1515/9781501508134-012.
Viehmann, S., Bau, M., Hoffmann, J.E., Münker, C., 2015. Geochemistry of the Krivoy Rog Banded Iron Formation, Ukraine, and the impact of peak episodes of increased global magmatic activity on the trace element composition of Precambrian seawater. Precambrian Res. 270, 165–180. https://doi.org/10.1016/j.precamres.2015.09.015.
Viehmann, S., Kujawa, R., Hohl, S.V., Tepe, N., Rodler, A.S., Hofmann, T., Draganits, E., 2023. Stromatolitic carbonates from the Middle Miocene of the western Pannonian Basin reflect trace metal availability in microbial habitats during the Badenian Salinity Crisis. Chem. Geol. 618, 121301 https://doi.org/10.1016/j.chemgeo.2023.121301.
Visscher, P.T., Reid, R.P., Bebout, B.M., 2000. Microscale observations of sulfate reduction: Correlation of microbial activity with lithified micritic laminae in modern marine stromatolites. Geology 28, 919–922. https://doi.org/10.1130/0091-7613(2000)28<919:MOOSRC>2.0.CO;2.
Vorlicek, T.P., Kahn, M.D., Kasuya, Y., Helz, G.R., 2004. Capture of molybdenum in pyrite-forming sediments: role of ligand-induced reduction by polysulfides 1 1Associate editor: M. Goldhaber. Geochim. Cosmochim. Acta 68, 547–556. https://doi.org/10.1016/S0016-7037(03)00444-7.
Walsh, M.W., 1992. Microfossils and possible microfossils from the early archean Onverwacht group, Barberton mountain land, South Africa. Precambrian Res. 54, 271–293. https://doi.org/10.1016/0301-9268(92)90074-X.
Walter, M.R., Buick, R., Dunlop, J.S.R., 1980. Stromatolites 3,400–3,500 Myr old from the North Pole area, Western Australia. Nature 284, 443–445. https://doi.org/10.1038/284443a0.
Warchola, T., Lalonde, S.V., Pecoits, E., von Gunten, K., Robbins, L.J., Alessi, D.S., Philippot, P., Konhauser, K.O., 2018. Petrology and geochemistry of the Boolgeeda Iron Formation, Hamersley Basin, Western Australia. Precambrian Res. 316, 155–173. https://doi.org/10.1016/j.precamres.2018.07.015.
Ward, D.M., Ferris, M.J., Nold, S.C., Bateson, M.M., 1998. A Natural View of Microbial Biodiversity within Hot Spring Cyanobacterial Mat Communities. Microbiol. Mol. Biol. Rev. 62, 1353–1370. https://doi.org/10.1128/MMBR.62.4.1353-1370.1998.
Webb, G.E., Kamber, B.S., 2000. Rare earth elements in Holocene reefal microbialites: a new shallow seawater proxy. Geochim. Cosmochim. Acta 64, 1557–1565. https://doi.org/10.1016/S0016-7037(99)00400-7.
Webby, B.D., 2002. Patterns of Ordovician Reef Development. In: Kiessling, W., Flügel, E., Golonka, J. (Eds.), Phanerozoic Reef Patterns. SEPM Society for Sedimentary Geology, p. 0. https://doi.org/10.2110/pec.02.72.0129.
Weber, J.N., 1965. Abstracts of papers submitted for six meetings with which the Society was associated. Geol. Soc. America. https://doi.org/10.1130/SPE82.
White, R.A., Wong, H.L., Ruvindy, R., Neilan, B.A., Burns, B.P., 2018. Viral Communities of Shark Bay Modern Stromatolites. Front. Microbiol. 9 https://doi.org/10.3389/fmicb.2018.01223.
White, R.A., Visscher, P.T., Burns, B.P., 2021. Between a Rock and a Soft Place: the Role of Viruses in Lithification of Modern Microbial Mats. Trends Microbiol. 29, 204–213. https://doi.org/10.1016/j.tim.2020.06.004.
Wilde, S.A., Valley, J.W., Peck, W.H., Graham, C.M., 2001. Evidence from detrital zircons for the existence of continental crust and oceans on the Earth 4.4 Gyr ago. Nature 409, 175–178. https://doi.org/10.1038/35051550.
Wille, M., Kramers, J.D., Nägler, T.F., Beukes, N.J., Schröder, S., Meisel, Th., Lacassie, J. P., Voegelin, A.R., 2007. Evidence for a gradual rise of oxygen between 2.6 and 2.5Ga from Mo isotopes and Re-PGE signatures in shales. Geochim. Cosmochim. Acta 71, 2417–2435. https://doi.org/10.1016/j.gca.2007.02.019.
Wille, M., Nebel, O., Van Kranendonk, M.J., Schoenberg, R., Kleinhanns, I.C., Ellwood, M.J., 2013. Mo–Cr isotope evidence for a reducing Archean atmosphere in 3.46–2.76Ga black shales from the Pilbara, Western Australia. Chem. Geol. 340, 68–76. https://doi.org/10.1016/j.chemgeo.2012.12.018.
Wilmeth, D.T., Johnson, H.A., Stamps, B.W., Berelson, W.M., Stevenson, B.S., Nunn, H.S., Grim, S.L., Dillon, M.L., Paradis, O., Corsetti, F.A., Spear, J.R., 2018. Environmental and Biological Influences on Carbonate Precipitation within Hot Spring Microbial Mats in Little Hot Creek, CA. Front. Microbiol. 9.
Wilmeth, D.T., Myers, K.D., Lalonde, S.V., Mänd, K., Konhauser, K.O., Grandin, P., van Zuilen, M.A., 2021. Evaporative silicification in floating microbial mats: patterns of oxygen production and preservation potential in silica-undersaturated streams, El Tatio, Chile. Geobiology 20, 310–330. https://doi.org/10.1111/gbi.12476.
Wilmeth, D.T., Lalonde, S.V., Berelson, W.M., Petryshyn, V., Celestian, A.J., Beukes, N.J., Awramik, S.M., Spear, J.R., Mahseredjian, T., Corsetti, F.A., 2022. Evidence for benthic oxygen production in Neoarchean lacustrine stromatolites. Geology 50, 907–911. https://doi.org/10.1130/G49894.1.
Zawaski, M.J., Kelly, N.M., Orlandini, O.F., Nichols, C.I.O., Allwood, A.C., Mojzsis, S.J., 2020. Reappraisal of purported ca. 3.7 Ga stromatolites from the Isua Supracrustal Belt (West Greenland) from detailed chemical and structural analysis. Earth Planet. Sci. Lett. 545, 116409 https://doi.org/10.1016/j.epsl.2020.116409.
Zeyen, N., Benzerara, K., Beyssac, O., Daval, D., Muller, E., Thomazo, C., Tavera, R., López-García, P., Moreira, D., Duprat, E., 2021. Integrative analysis of the mineralogical and chemical composition of modern microbialites from ten Mexican lakes: what do we learn about their formation? Geochim. Cosmochim. Acta 305, 148–184. https://doi.org/10.1016/j.gca.2021.04.030.
Zhong, S., Mucci, A., 1995. Partitioning of rare earth elements (REEs) between calcite and seawater solutions at 25°C and 1 atm, and high dissolved REE concentrations. Geochim. Cosmochim. Acta 59, 443–453. https://doi.org/10.1016/0016-7037(94)00381-U.